Infectious Disease Modelling 10 (2025) 207–228

Contents lists available at ScienceDirect

Infectious Disease Modelling

journal homepage: www.keaipublishing.com/idm

Dynamics of an SVEIR transmission model with protection awareness and two strains

Kaijing Chen [a], Fengying Wei [a, b, c, *], Xinyan Zhang [d, **], Hao Jin [d], Ruiyang Zhou [a], Yue Zuo [d], Kai Fan [d]

[a] School of Mathematics and Statistics, Fuzhou University, Fuzhou, 350116, Fujian, China
[b] Key Laboratory of Operations Research and Control of Universities in Fujian, Fuzhou University, Fuzhou, 350116, Fujian, China
[c] Center for Applied Mathematics of Fujian Province, Fuzhou University, Fuzhou, 350116, Fujian, China
[d] Jinzhou Center for Disease Control and Prevention, Jinzhou, 121000, Liaoning, China

ARTICLE INFO

Article history:
Received 19 July 2024
Received in revised form 30 September 2024
Accepted 1 October 2024
Available online 10 October 2024
Handling Editor: Dr Daihai He

Keywords:
SVEIR transmission model
Protection awareness
Two trains
Stability
Competitive exclusion

ABSTRACT

As of May 2024, the main strains of COVID-19 caused hundreds of millions of infection cases and millions of deaths worldwide. In this study, we consider the COVID-19 epidemics with the main strains in the Chinese mainland. We study complex interactions among hosts, non-pharmaceutical interventions, and vaccinations for the main strains by a differential equation model called SVEIR. The disease transmission model incorporates two strains and protection awareness of the susceptible population. Results of this study show that the protection awareness plays a crucial role against infection of the population, and that the vaccines are effective against the circulation of the earlier strains, but ineffective for emerging strains. By using the next generation matrix method, the basic reproduction number of the SVEIR model is firstly obtained. Our analysis by Hurwitz criterion and LaSalle's invariance principle shows that the disease free-equilibrium point is locally and globally asymptotically stable when the threshold value is below one. The existences of endemic equilibrium points are also established, and the global asymptotic stabilities are analyzed using the Lyapunov function method. Further, the SVEIR model is confirmed to satisfy the principle of competitive exclusion, of which the strain with the larger value of the basic reproduction number is dominant. Numerically, the surveillance data with the Omicron strain and the XBB strain are split by the cubic spline interpolation method. The fitting curves against the surveillance data are plotted using the least-squares method from MATLAB. The results indicate that the XBB strain dominates in this study. Moreover, a global sensitivity analysis of the key parameters is performed by using of PRCC. The numerical simulations imply that combination control strategy positively impacts on the infection scale than what separate control strategy does, and that the earlier time producing protection awareness for the public creates less infection scale, further that the increment of protection awareness also reduces the infection scale. Therefore, the policymakers of the local government are suggested to concern the changes of protection awareness of the public.

* Corresponding authors. School of Mathematics and Statistics, Fuzhou University, Fuzhou, 350116, Fujian, China.
** Corresponding author.
E-mail addresses: kj_dream@163.com (K. Chen), weifengying@fzu.edu.cn (F. Wei), pengyou_88888123@126.com (X. Zhang).
Peer review under responsibility of KeAi Communications Co., Ltd.

https://doi.org/10.1016/j.idm.2024.10.001

1. Introduction

Since COVID-19 was first detected in December 2019, WHO declared a public health emergency of international concern (PHEIC) which was the highest level of alarm on 30 January 2020, and classified COVID-19 as a pandemic on 11 March 2020 (World Health Drganization, 2020). As of 20 May 2024, COVID-19 had caused more than 7 billion infections and more than 7 million deaths worldwide (World Health Drganization, 2024). During the circulation of COVID-19, the non-pharmacological interventions (NPIs) were employed to slow down the infection scales at the early stage without the vaccines. The NPIs, including partial or total lockdowns, tracking and isolation of infected individuals, increasing social distances, wearing face masks (Guo et al., 2023; Zou, Fairley, et al., 2022), had the limited effects on stopping the pandemic, but it reduced the infection risks (Zhao et al., 2022). The vaccination gradually provided the protection for public to relax restrictions on human activities. However, new SARS-CoV-2 strain brokethrough the protection of the vaccines, and changed the situations of prevention and control (Garcia-Beltran et al., 2022; Lauring & Hodcroft, 2021).

The known SARS-CoV-2 strains include Alpha, Beta, Gamma, Delta, Omicron and XBB since the wild strain was detected in 2019 (Liu et al., 2023a, 2023b; Petrone et al., 2023; Shan et al., 2022; Sun et al., 2023), of which two or three strains might overlap simultaneously within an epidemic. In practice, compartmental models were usually applied to discover the long-term transmission dynamics of multiple strains. For instance, Tchoumi et al. (Tchoumi et al., 2022) derived the transmission dynamics for a two-strain model with vaccination for first-strain, and discussed the impacts of second-strain against the population with first-strain. When the incubation period was considered, Leon et al. (de Leon et al., 2022) investigated the two-strain model and the deployment of a vaccination program, aimed at the dynamics of two-strain infections including the varying transmission rates and responses to vaccines. Meanwhile, the competitive and exclusive relationship of two strains and the corresponding transmissions were worthy of investigation, of which the strain with larger basic reproduction number dominated in the population using the principle of competitive exclusion in Wang (Wang, 2022). Guo and Li (Guo & Li, 2023) developed a competitive model with Omicron strain and Delta strain, and then simulated the infection curves against the surveillance data from the United States, further derived the optimal control for the local government. Due to the differences of infection symptoms, Gao et al. (Gao et al., 2023) investigated a multi-strain model with distinct symptoms and NPIs, they derived the impacts of strain competition and control measures on the infection scale, simulation results showed that wearing masks prolonged the peak date. Moreover, Vashishth and Basaiti (Vashishth & Basaiti, 2024) developed a two-strain COVID-19 model of having thirteencompartments, and analyzed the impacts of non-pharmacological control measures, the impacts of imperfect and leaky vaccines on the infection scale and herd immunity.

The fact was that the coexistence of human beings and SARS-CoV-2 virus was persistent, and that NPIs triggered by the individuals' protection awareness still were workable for controlling the infection risk. The protection awareness mainly included media coverage on infectious diseases, the changes of individual behaviors, implementation of vaccines. In detail, the impacts of media coverage were investigated by adopting media influence factor to describe the spread and control of infectious diseases in a given area in Cui et al. (Cui et al., 2008). Later, the involvement of media coverage was described by using nonlinear contact functions in Li et al. (Li & Cui, 2009) and Sun et al. (Sun et al., 2011), the simulation results showed that media coverage could reduce the burden and the duration of the epidemics. In 2014, the choose of media functions determined the epidemic outcomes by comparing three different media functions in Collinson and Heffernan (Collinson & Heffernan, 2014). Meanwhile, the protection awareness was also reflected on the changes of individual behaviors. For instance, Xiao et al. (Yan et al., 2018) constructed the health belief model, and chose A/H1N1 and Ebola as typical examples to show that human behaviors played a key role in the spread of infectious diseases. Khatun et al. (Khatun et al., 2023) explored that high density of aware susceptible individuals created low density of treated individuals, and that both isolation and vaccination control were better than single control. Rai et al. (Kumar et al., 2019) combined public health awareness with the budgets, the results revealed that the positive publicity was benefitable for bacterial decline, the budget increasing was good for infection rate decreasing. In addition, implementation of vaccines was conducive to the suppression of infection scale. For instance, imperfect vaccination was extensively investigated using threshold strategies in Zhang and Xiao (Zhang & Xiao, 2020) and the effects of vaccination rates with time-varying transmission rates in Yu et al. (Yu et al., 2023).

This paper considers a two-strain compartmental model with protection awareness and vaccination, and the two-strain SVEIR model is applied to Jinzhou COVID-19 epidemic in Liaoning of China. The first concern is the expression of the basic reproduction number of two-strain model. Then, the stabilities of disease-free equilibrium point and infection equilibrium point are derived by constructing Laypunov functions. The competition and exclusion of two strains are also derived in Section 3. Combining with the surveillance data from the Jinzhou City, the data fittings by least squares method and global sensitivity analysis by PRCC are performed in Section 4. The impacts of protection awareness on the infection scales causing by two strains are analyzed in Section 5. Consequently, the main conclusions are obtained in Section 6.

2. Model formulation

Combined the features of surveillance data of Jinzhou COVID-19 epidemic and the previous studies including incubation period (Lan et al., 2024; Liu & Wei, 2022), vaccination (Chen et al., 2024; Li, Wei, & Mao, 2022; Lu & Wei, 2019; Wei et al., 2023), multi strains (Arruda et al., 2021; Cui & Liu, 2022; Wang et al., 2023) and protection awareness (Zhai et al., 2023), we will establish a two-strain SVEIR model, for describing the changes of Omicron strain and XBB strain on the Chinese mainland. The total population of Jinzhou City at time t is divided into seven compartments: the susceptible $S(t)$, the

vaccinated $V(t)$, the exposed with first-strain $E_1(t)$, the exposed with second-strain $E_2(t)$, the infected with first-strain $I_1(t)$, the infected with second-strain $I_2(t)$ and the recovered $R(t)$. In this study, we assume the following assumptions held: (i) The total population is homogeneously mixed. (ii) A vaccine is effective against first-strain, instead against second-strain. (iii) The vaccinated do not become the susceptible again (Andrews et al., 2022; Hall et al., 2022; Zhuang et al., 2022). (iv) The individuals are only infected by one strain. (v) The exposed has no effect on the spread of the virus (de Leon et al., 2022; Gonzalez-Parra et al., 2021; Vashishth & Basaiti, 2024). (vi) The recovered are regarded to be with temporary immunities and will not return to the susceptible. So, a two-strain SVEIR model with protection awareness is written as:

$$\begin{cases} \dot{S}(t) &= \Lambda - q\beta_1 SI_1 - q\beta_2 SI_2 - (1-q)(1-g)\beta_1 SI_1 - (1-q)(1-g)\beta_2 SI_2 - (\varphi+\mu)S, \\ \dot{V}(t) &= \varphi S - (1-a)\beta_1 VI_1 - \beta_2 VI_2 - \mu V, \\ \dot{E}_1(t) &= q\beta_1 SI_1 + (1-q)(1-g)\beta_1 SI_1 + (1-a)\beta_1 VI_1 - (\alpha_1+\mu)E_1, \\ \dot{E}_2(t) &= q\beta_2 SI_2 + (1-q)(1-g)\beta_2 SI_2 + \beta_2 VI_2 - (\alpha_2+\mu)E_2, \\ \dot{I}_1(t) &= \alpha_1 E_1 - (\gamma_1+\mu_1+\mu)I_1, \\ \dot{I}_2(t) &= \alpha_2 E_2 - (\gamma_2+\mu_2+\mu)I_2, \\ \dot{R}(t) &= \gamma_1 I_1 + \gamma_2 I_2 - \mu R. \end{cases} \tag{1}$$

In model (1), Λ is the natural recruitment; β_1, the infection rate of first-strain; β_2, the infection rate of second-strain. Due to the fact that the susceptible with the protection awareness will protect themselves effectively, the interactions with the infected are assumed to be the rate of $(1-q)(1-g)\beta_1$, where q is the percentage of the susceptible without protection awareness, g is the protection efficiency that means the proportion of the susceptible with protection awareness efficiently avoid the infection, $1-g$ represents the rate of protection failure that the susceptible with protection awareness are being infected. Here, φ is the vaccination rate; a is vaccine efficacy; α_1 and α_2 are mean incubation periods for first-strain and second-strain; γ_1 and γ_2 are the average recovery rates for first-strain and second-strain; μ is natural death rate; μ_1 and μ_2, the disease-incuced death rates by first-strain and second-strain. The flow diagram of model (1) is shown in Fig. 1.

3. Mathematical analysis

Theorem 3.1. *The closed set* $\Omega = \{(S,V,E_1,E_2,I_1,I_2,R) \in \mathbb{R}^7_+ : N \le \frac{\Lambda}{\mu}\}$ *is positively invariant for model* (1).

Proof If $E_1(t)=0$, then $\dot{I}_{1|I_1=0} = \alpha_1 E_1 = 0$, which gives that I_1 is a positive constant. We then get $\dot{E}_{1|E_1=0} = q\beta_1 SI_1 + (1-q)(1-g)\beta_1 SI_1 + (1-a)\beta_1 VI_1 > 0$. If $E_1(t)>0$, then $\dot{I}_{1|I_1=0} = \alpha_1 E_1 > 0$, which gives that I_1 is also a positive constant. We then get $\dot{E}_{1|E_1=0} = q\beta_1 SI_1 + (1-q)(1-g)\beta_1 SI_1 + (1-a)\beta_1 VI_1 > 0$. By the similar discussions, the processing of $\dot{E}_{2|E_2=0}$ and $\dot{I}_{2|I_2=0}$ can be conducted in a similar manner. Since $\dot{S}_{|S=0} = \Lambda > 0$, $\dot{V}_{|V=0} = \varphi S > 0$, $\dot{E}_{1|E_1=0} > 0$, $\dot{E}_{2|E_2=0} > 0$, $\dot{I}_{1|I_1=0} > 0$, $\dot{I}_{2|I_2=0} > 0$, $\dot{R}_{|R=0} = \gamma_1 I_1 + \gamma_2 I_2 > 0$, then the solution of model (1) is non-negative.

Consider a new variable $T = S+V+E_1+E_2+I_1+I_2+R-\frac{\Lambda}{\mu}$, adding all equations of model (1), then T satisfies:

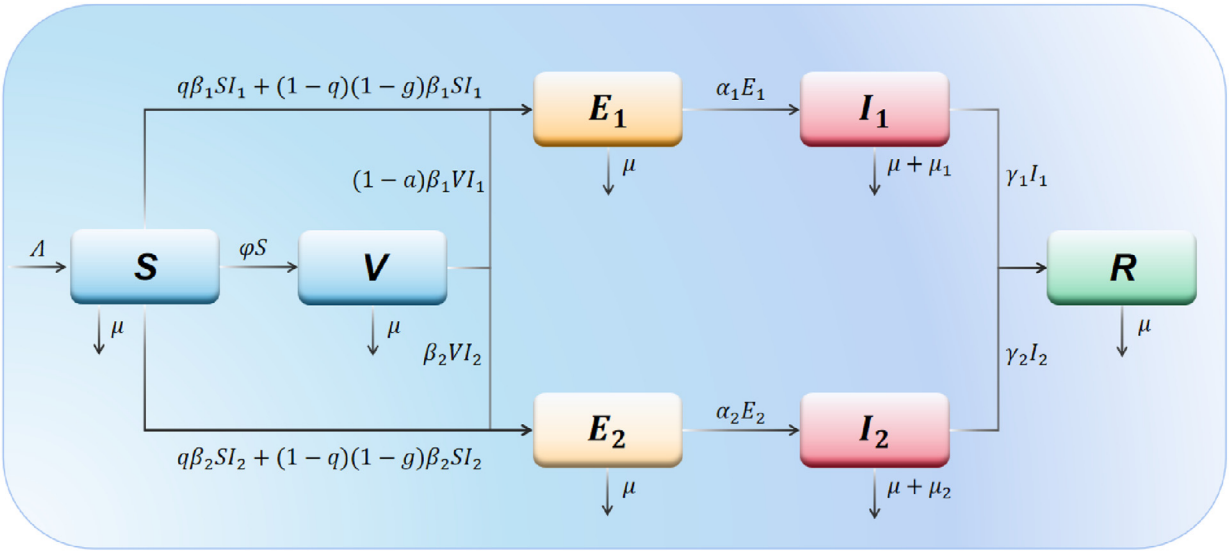

Fig. 1. Flow diagram of the local population exposed to two strains of COVID-19.

$$\begin{aligned}\dot{T} &= \dot{S}+\dot{V}+\dot{E_1}+\dot{E_2}+\dot{I_1}+\dot{I_2}+\dot{R}\\ &= \Lambda-\mu(S+V+E_1+E_2+I_1+I_2+R)-\mu_1R-\mu_2R\\ &\le \Lambda-\mu(S+V+E_1+E_2+I_1+I_2+R)\\ &\le \mu\left[\frac{\Lambda}{\mu}-(S+V+E_1+E_2+I_1+I_2+R)\right]\\ &= -\mu T.\end{aligned}$$

Hence

$$T(t)\le T(0)e^{-\mu t}. \tag{2}$$

Since all variables are non-negative and bounded, set Ω is positively invariant for model (1). □

Theorem 3.2. *The disease-free equilibrium point (DEEP) of model (1) is given by* $P_0=(S_0, V_0, 0, 0, 0, 0, 0)$ *where* $S_0=\frac{\Lambda}{\mu+\varphi}$ *and* $V_0=\frac{\Lambda\varphi}{\mu(\mu+\varphi)}$. *The basic reproduction number is* $\mathcal{R}_0=\max\{\mathcal{R}_0^1,\mathcal{R}_0^2\}$ *with*

$$\mathcal{R}_0^1=\frac{\alpha_1\Lambda[q\beta_1\mu+(1-q)(1-g)\beta_1\mu+(1-a)\beta_1\varphi]}{\mu(\mu+\varphi)(\alpha_1+\mu)(\gamma_1+\mu_1+\mu)},$$

$$\mathcal{R}_0^2=\frac{\alpha_2\Lambda[q\beta_2\mu+(1-q)(1-g)\beta_2\mu+\beta_2\varphi]}{\mu(\mu+\varphi)(\alpha_2+\mu)(\gamma_2+\mu_2+\mu)}.$$

Proof Let the first-strain subsystem

$$\begin{cases}\dot{S}(t) &= \Lambda-q\beta_1SI_1-(1-q)(1-g)\beta_1SI_1-(\varphi+\mu)S,\\ \dot{V}(t) &= \varphi S-(1-a)\beta_1VI_1-\mu V,\\ \dot{E}_1(t) &= q\beta_1SI_1+(1-q)(1-g)\beta_1SI_1+(1-a)\beta_1VI_1-(\alpha_1+\mu)E_1,\\ \dot{I}_1(t) &= \alpha_1E_1-(\gamma_1+\mu_1+\mu)I_1,\\ \dot{R}(t) &= \gamma_1I_1-\mu R.\end{cases} \tag{3}$$

The DEEP is $P_0=(\frac{\Lambda}{\mu+\varphi},\frac{\Lambda\varphi}{\mu(\mu+\varphi)},0,0,0)$. Set

$$\begin{aligned}\dot{E}_1(t) &= \mathcal{F}_1(S(t),V(t),E_1(t),I_1(t))-\mathcal{V}_1(S(t),V(t),E_1(t),I_1(t))\\ &= (q\beta_1SI_1+(1-q)(1-g)\beta_1SI_1+(1-a)\beta_1VI_1)-[(\alpha_1+\mu)E_1],\\ \dot{I}_1(t) &= \mathcal{F}_2(S(t),V(t),E_1(t),I_1(t))-\mathcal{V}_2(S(t),V(t),E_1(t),I_1(t))\\ &= 0-[-\alpha_1E_1+(\gamma_1+\mu_1+\mu)I_1].\end{aligned}$$

Thus, we obtain

$$F=\begin{pmatrix}\frac{\partial\mathcal{F}_1}{\partial E_1} & \frac{\partial\mathcal{F}_1}{\partial I_1}\\ \frac{\partial\mathcal{F}_2}{\partial E_1} & \frac{\partial\mathcal{F}_2}{\partial I_1}\end{pmatrix}=\begin{pmatrix}0 & q\beta_1S+(1-q)(1-g)\beta_1S+(1-a)\beta_1V\\ 0 & 0\end{pmatrix},$$

$$V=\begin{pmatrix}\frac{\partial\mathcal{V}_1}{\partial E_1} & \frac{\partial\mathcal{V}_1}{\partial I_1}\\ \frac{\partial\mathcal{V}_2}{\partial E_1} & \frac{\partial\mathcal{V}_2}{\partial I_1}\end{pmatrix}=\begin{pmatrix}\alpha_1+\mu & 0\\ -\alpha_1 & \gamma_1+\mu_1+\mu\end{pmatrix},$$

which gives

$$V^{-1}=\begin{pmatrix}\frac{1}{\alpha_1+\mu} & 0\\ \frac{\alpha_1}{(\gamma_1+\mu_1+\mu)(\alpha_1+\mu)} & \frac{1}{\gamma_1+\mu_1+\mu}\end{pmatrix}.$$

The next generation matrix in (van den Driessche & Watmough, 2002) is defined as $M=FV^{-1}$, that was

$$M = \begin{pmatrix} \dfrac{\alpha_1[q\beta_1 S + (1-q)(1-g)\beta_1 S + (1-a)\beta_1 V]}{(\gamma_1+\mu_1+\mu)(\alpha_1+\mu)} & \dfrac{q\beta_1 S + (1-q)(1-g)\beta_1 S + (1-a)\beta_1 V}{\gamma_1+\mu_1+\mu} \\ 0 & 0 \end{pmatrix}.$$

Since the spectral radius of M is defined as the basic reproduction number $\mathcal{R}_0^1$, we obtain the specific expression of first-strain

$$\begin{aligned} \mathcal{R}_0^1 &= \frac{\alpha_1[q\beta_1 S_0 + (1-q)(1-g)\beta_1 S_0 + (1-a)\beta_1 V_0]}{(\gamma_1+\mu_1+\mu)(\alpha_1+\mu)} \\ &= \frac{\alpha_1\Lambda[q\beta_1\mu + (1-q)(1-g)\beta_1\mu + (1-a)\beta_1\varphi]}{\mu(\mu+\varphi)(\alpha_1+\mu)(\gamma_1+\mu_1+\mu)}. \end{aligned} \tag{4}$$

From the similar discussion, the basic reproduction number of the second-strain $\mathcal{R}_0^2$ is

$$\mathcal{R}_0^2 = \frac{\alpha_2\Lambda[q\beta_2\mu + (1-q)(1-g)\beta_2\mu + \beta_2\varphi]}{\mu(\mu+\varphi)(\alpha_2+\mu)(\gamma_2+\mu_2+\mu)}. \tag{5}$$

Then, the basic reproduction number of model (1) is $\mathcal{R}_0 = \max\{\mathcal{R}_0^1, \mathcal{R}_0^2\}$. □

Theorem 3.3. *The DEEP P_0 is unstable if $\mathcal{R}_0 > 1$ while it is locally asymptotically stable if $\mathcal{R}_0 < 1$.*

Proof The Jacobian matrix associate with model (1) at DEEP J_{P_0} is given by

$$J_{P_0} = \begin{pmatrix} -(\varphi+\mu) & 0 & 0 & 0 & A\beta_1 S_0 & A\beta_2 S_0 \\ \varphi & -\mu & 0 & 0 & (1-a)\beta_1 V_0 & \beta_2 V_0 \\ 0 & 0 & -(\alpha_1+\mu) & 0 & A\beta_1 S_0 + (1-a)\beta_1 V_0 & 0 \\ 0 & 0 & 0 & -(\alpha_2+\mu) & 0 & A\beta_2 S_0 + \beta_2 V_0 \\ 0 & 0 & -\alpha_1 & 0 & \gamma_1+\mu_1+\mu & 0 \\ 0 & 0 & 0 & -\alpha_2 & 0 & \gamma_2+\mu_2+\mu \end{pmatrix}, \tag{6}$$

with $A = q + (1-q)(1-g)$. Thus, the eigenvalues of J_{P_0} are $\lambda_1 = -\mu < 0$, $\lambda_2 = -(\varphi+\mu) < 0$, and other four eigenvalues corresponding to the sub-matrix

$$\begin{pmatrix} -(\alpha_1+\mu) & 0 & A\beta_1 S_0 + (1-a)\beta_1 V_0 & 0 \\ 0 & -(\alpha_2+\mu) & 0 & A\beta_2 S_0 + \beta_2 V_0 \\ -\alpha_1 & 0 & \gamma_1+\mu_1+\mu & 0 \\ 0 & -\alpha_2 & 0 & \gamma_2+\mu_2+\mu \end{pmatrix}$$

are computed by the characteristic equation

$$\begin{aligned} P(\lambda) &= \left[\lambda^2 + (2\mu+\alpha_1+\gamma_1+\mu_1)\lambda + \left(1-\mathcal{R}_0^1\right)(\gamma_1+\mu_1+\mu)(\alpha_1+\mu)\right] \\ &\times \left[\lambda^2 + (2\mu+\alpha_2+\gamma_2+\mu_2)\lambda + \left(1-\mathcal{R}_0^2\right)(\gamma_2+\mu_2+\mu)(\alpha_2+\mu)\right] = 0. \end{aligned}$$

If $\mathcal{R}_0^1 < 1$ and $\mathcal{R}_0^2 < 1$, then the roots of $P(\lambda)$ have negative real parts. We obtain that if $\mathcal{R}_0 < 1$, DEEP P_0 of model (1) is locally asymptotically stable. If $\mathcal{R}_0 > 1$, then DEEP P_0 loses its stability. □

Theorem 3.4. *The DEEP P_0 is globally asymptotically stable if $\mathcal{R}_0 < 1$.*

Proof Consider the Lyapunov function

$$W(S, V, E_1, E_2, I_1, I_2) = \alpha_1 E_1 + (\alpha_1+\mu) I_1 + \alpha_2 E_2 + (\alpha_2+\mu) I_2, \tag{7}$$

which yields that $W(S, V, E_1, E_2, I_1, I_2) > 0$ due to $E_1, E_2, I_1, I_2 > 0$, and $W(S, V, E_1, E_2, I_1, I_2)$ attains zero at $E_1 = E_2 = I_1 = I_2 = 0$. The time-derivative of W is given by:

$$\begin{aligned}
\dot{W} &= \alpha_1\dot{E_1} + (\alpha_1+\mu)\dot{I_1} + \alpha_2\dot{E_2} + (\alpha_2+\mu)\dot{I_2} \\
&= \alpha_1[q\beta_1 SI_1 + (1-q)(1-g)\beta_1 SI_1 + (1-a)\beta_1 VI_1 - (\alpha_1+\mu)E_1] + (\alpha_1+\mu)[\alpha_1 E_1 - (\gamma_1+\mu_1+\mu)I_1] \\
&\quad +\alpha_2[q\beta_2 SI_2 + (1-q)(1-g)\beta_2 SI_2 + \beta_2 VI_2 - (\alpha_2+\mu)E_2] + (\alpha_2+\mu)[\alpha_2 E_2 - (\gamma_2+\mu_2+\mu)I_2] \\
&= \alpha_1[q\beta_1 SI_1 + (1-q)(1-g)\beta_1 SI_1 + (1-a)\beta_1 VI_1] - (\alpha_1+\mu)(\gamma_1+\mu_1+\mu)I_1 \\
&\quad +\alpha_2[q\beta_2 SI_2 + (1-q)(1-g)\beta_2 SI_2 + \beta_2 VI_2] - (\alpha_2+\mu)(\gamma_2+\mu_2+\mu)I_2 \\
&= (\alpha_1+\mu)(\gamma_1+\mu_1+\mu)I_1\left[\frac{\alpha_1[q\beta_1 S + (1-q)(1-g)\beta_1 S + (1-a)\beta_1 V]}{(\gamma_1+\mu_1+\mu)(\alpha_1+\mu)} - 1\right] \\
&\quad +(\alpha_2+\mu)(\gamma_2+\mu_2+\mu)I_2\left[\frac{\alpha_2[q\beta_2 S + (1-q)(1-g)\beta_2 S + \beta_2 V]}{(\gamma_2+\mu_2+\mu)(\alpha_2+\mu)} - 1\right].
\end{aligned}$$

Due to $S \le S_0$ and $V \le V_0$, we then get

$$\dot{W} \le (\alpha_1+\mu)(\gamma_1+\mu_1+\mu)I_1(\mathcal{R}_0^1 - 1) + (\alpha_2+\mu)(\gamma_2+\mu_2+\mu)I_2(\mathcal{R}_0^2 - 1). \tag{8}$$

Furthermore,$\dot{W} = 0$ if and only if $E_1 = E_2 = I_1 = I_2 = 0$, by using LaSalle's invariance principle, this implies that P_0 is globally asymptotically stable in Ω. □

We denote that S_{FS}^* and V_{FS}^* represent the numbers of susceptible individuals and vaccinated individuals, respectively, at the infection equilibrium point (IEP) when the first-strain is dominant. The similar interpretation can be applied to the situation where the second-strain is dominant, of which S_{SS}^* and V_{SS}^* represent the numbers of susceptible individuals and vaccinated individuals, respectively.

Theorem 3.5. *Model* (1) *has*

(i) *a unique first-strain IEP* $P_1 = (S_{FS}^*, V_{FS}^*, E_1^*, 0, I_1^*, 0, R^*)$ *if and only if* $\mathcal{R}_0^1 > 1$.
(ii) *a unique second-strain IEP* $P_2 = (S_{SS}^*, V_{SS}^*, 0, E_2^*, 0, I_2^*, R^*)$ *if and only if* $\mathcal{R}_0^2 > 1$.
(iii) *a two-strain IEP* $P_3 = (S^*, V^*, E_1^*, E_2^*, I_1^*, I_2^*, R^*)$ *if and only if* $\mathcal{R}_0^1 > 1$ *and* $\mathcal{R}_0^2 > 1$.

Proof (i) An equilibrium point for subsystem (3) satisfies, with $A = q + (1-q)(1-g)$.

$$\begin{cases}
0 = \Lambda - A\beta_1 SI_1 - (\varphi+\mu)S, \\
0 = \varphi S - (1-a)\beta_1 VI_1 - \mu V, \\
0 = A\beta_1 SI_1 + (1-a)\beta_1 VI_1 - (\alpha_1+\mu)E_1, \\
0 = \alpha_1 E_1 - (\gamma_1+\mu_1+\mu)I_1, \\
0 = \gamma_1 I_1 - \mu R,
\end{cases} \tag{9}$$

which reduces to

$$\begin{cases}
S_{FS}^* &= \dfrac{\Lambda}{A\beta_1 I_1^* + (\varphi+\mu)}, \\
V_{FS}^* &= \dfrac{\varphi S_{FS}^*}{(1-a)\beta_1 I_1^* + \mu}, \\
E_1^* &= \dfrac{A\beta_1 S_{FS}^* I_1^* + (1-a)\beta_1 V_{FS}^* I_1^*}{\alpha_1+\mu}, \\
I_1^* &= \dfrac{\alpha_1 E_1^*}{\gamma_1+\mu_1+\mu}, \\
R^* &= \dfrac{\gamma_1 I_1^*}{\mu}.
\end{cases} \tag{10}$$

From the fourth equality (10), one deduces that

$$I_1^* = \alpha_1 \Lambda \frac{[(1-a)\beta_1 I_1^* + \mu]A\beta_1 I_1^* + \varphi(1-a)\beta_1 I_1^*}{[(1-a)\beta_1 I_1^* + \mu][A\beta_1 I_1^* + (\varphi+\mu)](\alpha_1+\mu)(\gamma_1+\mu_1+\mu)}. \tag{11}$$

If $I_1^* = 0$ then $S_{FS}^* = \frac{\Lambda}{\mu+\varphi}$, $V_{FS}^* = \frac{\Lambda\varphi}{\mu(\mu+\varphi)}$, $E_1^* = 0$, $R^* = 0$. This equilibrium knows as the DEEP P_0 in Theorem 3.2. If $I_1^* \neq 0$, then define

$$h(I_1^*) = 1 - \alpha_1 \Lambda \frac{[(1-a)\beta_1 I_1^* + \mu]A\beta_1 + \varphi(1-a)\beta_1}{[(1-a)\beta_1 I_1^* + \mu][A\beta_1 I_1^* + (\varphi+\mu)](\alpha_1+\mu)(\gamma_1+\mu_1+\mu)}. \tag{12}$$

The derivative of h is given by

$$\dot{h}(I_1^*) = \frac{-\alpha_1 \Lambda (B_1 - B_2 B_3)}{[(1-a)\beta_1 I_1^* + \mu]^2 [A\beta_1 I_1^* + (\varphi+\mu)]^2 (\alpha_1+\mu)(\gamma_1+\mu_1+\mu)},$$

with

$$\begin{aligned} B_1 &= (1-a)A\beta_1^2 [(1-a)\beta_1 I_1^* + \mu]\,[A\beta_1 I_1^* + (\varphi+\mu)], \\ B_2 &= (1-a)\beta_1 [A\beta_1 I_1^* + (\varphi+\mu)] + [(1-a)\beta_1 I_1^* + \mu]A\beta_1, \\ B_3 &= [(1-a)\beta_1 I_1^* + \mu]A\beta_1 + (1-a)\beta_1\varphi. \end{aligned}$$

After the simplification for $\dot{h}(I_1^*)$, which is concluded that

$$\dot{h}(I_1^*) = \frac{\alpha_1 \Lambda B_4}{[(1-a)\beta_1 I_1^* + \mu]^2 [A\beta_1 I_1^* + (\varphi+\mu)]^2 (\alpha_1+\mu)(\gamma_1+\mu_1+\mu)} > 0, \tag{13}$$

with

$$\begin{aligned} B_4 &= [(1-a)\beta_1]^2 (A\beta_1)^2 {I_1^*}^2 \\ &\quad + 2[(1-a)\beta_1]A\beta_1 [(1-a)\beta_1\varphi + (A\beta_1)\mu] I_1^* \\ &\quad + [(1-a)\beta_1]^2 \varphi(\varphi+\mu) + (A\beta_1)^2\mu^2 + [(1-a)\beta_1]A\beta_1\mu\varphi > 0. \end{aligned}$$

Since all parameters are non-negative, one can easily deduce that the function h is an increasing function. A simple computation gives

$$\begin{aligned} \lim_{I_1^* \to 0} h(I_1^*) &= 1 - \frac{\alpha_1 \Lambda \left[(1-a)\beta_1 \lim\limits_{I_1^* \to 0} I_1^* + \mu\right] A\beta_1 + \varphi(1-a)\beta_1}{\left[(1-a)\beta_1 \lim\limits_{I_1^* \to 0} I_1^* + \mu\right]\left[A\beta_1 \lim\limits_{I_1^* \to 0} I_1^* + (\varphi+\mu)\right](\alpha_1+\mu)(\gamma_1+\mu_1+\mu)} \\ &= 1 - \frac{\Lambda\alpha_1 [A\beta_1 S_0 + (1-a)\beta_1 V_0]}{\mu(\varphi+\mu)(\alpha_1+\mu)(\gamma_1+\mu_1+\mu)} \\ &= 1 - \mathcal{R}_0^1, \end{aligned}$$

and

$$
\begin{aligned}
h\left(\frac{\Lambda}{\mu}\right) &= 1-\alpha_1\Lambda\frac{\left[(1-a)\beta_1\frac{\Lambda}{\mu}+\mu\right]A\beta_1+\varphi(1-a)\beta_1}{\left[(1-a)\beta_1\frac{\Lambda}{\mu}+\mu\right]\left[A\beta_1\frac{\Lambda}{\mu}+(\varphi+\mu)\right](\alpha_1+\mu)(\gamma_1+\mu_1+\mu)}\\
&> 1-\alpha_1\Lambda\frac{\left[(1-a)\beta_1\frac{\Lambda}{\mu}+\mu\right]A\beta_1+\varphi(1-a)\beta_1}{\left[(1-a)\beta_1\frac{\Lambda}{\mu}+\mu\right]\left[A\beta_1\frac{\Lambda}{\mu}+(\varphi+\mu)\right]\alpha_1\mu}\\
&= \frac{(1-a)\beta_1\Lambda+\mu^2+\varphi\mu}{\left[(1-a)\beta_1\frac{\Lambda}{\mu}+\mu\right]\left[A\beta_1\frac{\Lambda}{\mu}+(\varphi+\mu)\right]}>0.
\end{aligned}
$$

By $\mathcal{R}_0^1>1$, $\lim_{I_1^*\to 0}h(I_1^*)<0$ and $h(\frac{\Lambda}{\mu})>0$, $h(I_1)$ admits a unique solution I_1^* in $(0,\frac{\Lambda}{\mu})$. The uniqueness of $P_1=(S_{FS}^*,V_{FS}^*,E_1^*,0,I_1^*,0,R^*)$ holds.

(ii) The proof follows the same approach and steps as does in Case (i).

(iii) To compute P_3, let $x_1^*=\beta_1 I_1^*$, $x_2^*=\beta_2 I_2^*$. Solution of model (1) at P_3 satisfies:

$$
\begin{cases}
\Lambda-Ax_1^*S^*-Ax_2^*S^*-(\varphi+\mu)S=0,\\
\varphi S^*-(1-a)x_1^*V^*-x_2^*V^*-\mu V=0,\\
Ax_1^*S^*+(1-a)x_1^*V^*-(\alpha_1+\mu)E_1^*=0,\\
Ax_2^*S^*+x_2^*V^*-(\alpha_2+\mu)E_2^*=0,\\
\alpha_1E_1^*-(\gamma_1+\mu_1+\mu)I_1^*=0,\\
\alpha_2E_2^*-(\gamma_2+\mu_2+\mu)I_2^*=0,
\end{cases}
\tag{14}
$$

The following expressions are obtained from equality (14) that

$$
\begin{aligned}
S^* &= \frac{\Lambda}{Ax_1^*+Ax_2^*+\mu+\varphi},\\
V^* &= \frac{\varphi\Lambda}{\left[(1-a)x_1^*+x_2^*+\mu\right](Ax_1^*+Ax_2^*+\mu+\varphi)},\\
E_1^* &= \frac{\Lambda Ax_1^*\left[(1-a)x_1^*+x_2^*+\mu\right]+(1-a)x_1^*\varphi\Lambda}{(\alpha_1+\mu)\left[(1-a)x_1^*+x_2^*+\mu\right](Ax_1^*+Ax_2^*+\mu+\varphi)},\\
E_2^* &= \frac{\Lambda Ax_2^*\left[(1-a)x_1^*+x_2^*+\mu\right]+x_2^*\varphi\Lambda}{(\alpha_2+\mu)\left[(1-a)x_1^*+x_2^*+\mu\right](Ax_1^*+Ax_2^*+\mu+\varphi)},\\
I_1^* &= \frac{\alpha_1\Lambda Ax_1^*\left[(1-a)x_1^*+x_2^*+\mu\right]+\alpha_1(1-a)x_1^*\varphi\Lambda}{(\gamma_1+\mu_1+\mu)(\alpha_1+\mu)\left[(1-a)x_1^*+x_2^*+\mu\right](Ax_1^*+Ax_2^*+\mu+\varphi)},\\
I_2^* &= \frac{\alpha_2\Lambda Ax_2^*\left[(1-a)x_1^*+x_2^*+\mu\right]+\alpha_2x_2^*\varphi\Lambda}{(\gamma_2+\mu_2+\mu)(\alpha_2+\mu)\left[(1-a)x_1^*+x_2^*+\mu\right](Ax_1^*+Ax_2^*+\mu+\varphi)}.
\end{aligned}
\tag{15}
$$

Substituting the expressions of (15) into $x_1^*=\beta_1 I_1^*$ and $x_2^*=\beta_2 I_2^*$, which yields the following equality:

$$\begin{aligned}(1-a)BAx_1^{*2}+BAx_2^{*2}+(2-a)BAx_1^*x_2^*+\left[CB\left(1-\mathcal{R}_0^1\right)+\mu BA+D\right]x_1^* &= \\ +\left[PB\left(1-\mathcal{R}_0^1\right)+\mu BA+F\right]x_2^*+\mu PB\left(1-\mathcal{R}_0^1\right) &= 0\end{aligned} \tag{16}$$

$$\begin{aligned}(1-a)GAx_1^{*2}+GAx_2^{*2}+(2-a)GAx_1^*x_2^*+\left[CG\left(1-\mathcal{R}_0^2\right)+\mu GA+H\right]x_1^* &= \\ +\left[PG\left(1-\mathcal{R}_0^2\right)+\mu GA+Q\right]x_2^*+\mu PG\left(1-\mathcal{R}_0^2\right) &= 0,\end{aligned} \tag{17}$$

where

$$\begin{aligned}&B=(\gamma_1+\mu_1+\mu)(\alpha_1+\mu),C=(1-a)(\mu+\varphi),\\ &D=\frac{(1-a)^2}{\mu}\alpha_1\beta_1\varphi\Lambda,P=\mu+\varphi,F=\frac{1-a}{\mu}\alpha_1\beta_1\varphi\Lambda\\ &G=(\gamma_2+\mu_2+\mu)(\alpha_2+\mu),H=\frac{1-a}{\mu}\alpha_2\beta_2\varphi\Lambda,Q=\frac{1}{\mu}\alpha_2\beta_2\varphi\Lambda.\end{aligned} \tag{18}$$

Since the constant terms in (16) and (17) are negative when $\mathcal{R}_0^1>1$ and $\mathcal{R}_0^2>1$, all other coefficients can be positive. Therefore, (16) and (17) have a positive solution for $\mathcal{R}_0^1>1$ and $\mathcal{R}_0^2>1$. The proof is complete. □

Theorem 3.6. *Let $\mathcal{R}_0^1>1$. Then the unique first-strain IEP P_1 of model* (3) *is globally asymptotically stable in* Ω.

Proof Consider the first-strain IEP $P_1=(S_{FS}^*,V_{FS}^*,E_1^*,0,I_1^*,0,R^*)$, where S_{FS}^*, V_{FS}^*, E_1^*, I_1^*, R^* satisfy the following relations:

$$\varphi S_{FS}^*=(1-a)\beta_1V_{FS}^*I_1^*+\mu V_{FS}^*, \tag{19}$$

$$\Lambda=\mu S_{FS}^*+\mu V_{FS}^*+(1-a)\beta_1V_{FS}^*I_1^*+A\beta_1S_{FS}^*I_1^*, \tag{20}$$

$$(\mu+\alpha_1)E_1^*=(1-a)\beta_1V_{FS}^*I_1^*+A\beta_1S_{FS}^*I_1^*, \tag{21}$$

$$(\mu+\alpha_1)(\gamma_1+\mu_1+\mu)=\alpha_1(1-a)\beta_1V_{FS}^*+A\alpha\beta_1S_{FS}^*. \tag{22}$$

In order to prove the global asymptotic stability of P_1, let the Lyapunov function:

$$W_1=S-S_{FS}^*-S_{FS}^*\ln\frac{S}{S_{FS}^*}+V-V_{FS}^*-V_{FS}^*\ln\frac{V}{V_{FS}^*}+E_1-E_1^*-E_1^*\ln\frac{E_1}{E_1^*}+\frac{\alpha_1+\mu}{\alpha_1}\left(I_1-I_1^*-I_1^*\ln\frac{I_1}{I_1^*}\right).$$

The time-derivative of W_1, along solutions of model (1) is given by

$$\begin{aligned}\dot{W}_1 &= \left(1-\frac{S_{FS}^*}{S}\right)\dot{S}+\left(1-\frac{V_{FS}^*}{V}\right)\dot{V}+\left(1-\frac{E_1^*}{E_1}\right)\dot{E_1}+\frac{\alpha_1+\mu}{\alpha_1}\left(1-\frac{I_1^*}{I_1}\right)\dot{I_1}\\ &= \left(1-\frac{S_{FS}^*}{S}\right)[\Lambda-A\beta_1SI_1-(\varphi+\mu)S]+\left(1-\frac{V_{FS}^*}{V}\right)[\varphi S-(1-a)\beta_1VI_1-\mu V]\\ &\quad+\left(1-\frac{E_1^*}{E_1}\right)[A\beta_1SI_1+(1-a)\beta_1VI_1-(\alpha_1+\mu)E_1]\\ &\quad+\frac{\alpha_1+\mu}{\alpha_1}\left(1-\frac{I_1^*}{I_1}\right)[\alpha_1E_1-(\gamma_1+\mu_1+\mu)I_1].\end{aligned}$$

Together with (19)–(22), we have

$$\begin{aligned}\dot{W}_1 &= \mu S^*_{FS}\left(2-\frac{S}{S^*_{FS}}-\frac{S^*_{FS}}{S}\right)+\mu V^*_{FS}\left(3-\frac{S^*_{FS}}{S}-\frac{V}{V^*_{FS}}-\frac{S}{S^*_{FS}}\frac{V^*_{FS}}{V}\right)\\ &+A\beta_1 S^*_{FS}I^*_1\left(3-\frac{S^*_{FS}}{S}-\frac{I_1}{I^*_1}\frac{S}{S^*_{FS}}\frac{E^*_1}{E_1}-\frac{E_1}{E^*_1}\frac{I^*_1}{I_1}\right)\\ &+(1-a)\beta_1 V^*_1 I^*_1\left(4-\frac{S}{S^*_{FS}}\frac{V^*_{FS}}{V}-\frac{I_1}{I^*_1}\frac{V}{V^*_{FS}}\frac{E^*_1}{E_1}-\frac{E_1}{E^*_1}\frac{I^*_1}{I_1}-\frac{S^*_{FS}}{S}\right).\end{aligned}$$

Since $x_1+x_2+\cdots+x_n \geq n\sqrt[n]{x_1x_2\cdots x_n}\quad x_1,x_2,\ldots,x_n \geq 0$, then

$$\begin{aligned}&2-\frac{S}{S^*_{FS}}-\frac{S^*_{FS}}{S}\leq 0\\ &3-\frac{S^*_{FS}}{S}-\frac{V}{V^*_{FS}}-\frac{S}{S^*_{FS}}\frac{V^*_{FS}}{V}\leq 0\\ &3-\frac{S^*_{FS}}{S}-\frac{I_1}{I^*_1}\frac{S}{S^*_{FS}}\frac{E^*_1}{E_1}-\frac{E_1}{E^*_1}\frac{I^*_1}{I_1}\leq 0\\ &4-\frac{S}{S^*_{FS}}\frac{V^*_{FS}}{V}-\frac{I_1}{I^*_1}\frac{V}{V^*_{FS}}\frac{E^*_1}{E_1}-\frac{E_1}{E^*_1}\frac{I^*_1}{I_1}-\frac{S^*_{FS}}{S}\leq 0.\end{aligned}$$

Therefore $\dot{W}_1 \leq 0$. Because of Lyapunov theorem, P_1 is stable. Moreover, $\dot{W}_1 = 0$ if and only if $S = S^*_{FS}, V = V^*_{FS}, I_1 = I^*_1, E_1 = E^*_1$. Further, it can be proved that $M_1 = \{P_1\}$ is the largest compact invariant subset of $\left\{(S,V,E_1,E_2,I_1,I_2,R)\in\Omega : \dot{W}_1 = 0\right\}$. By LaSalle's invariance principle, the endemic equilibrium point P_1 of model (1) is globally asymptotically stable. □

Theorem 3.7. *Let $\mathcal{R}^1_0 > 1, \mathcal{R}^2_0 > 1$. Then a both-strain IEP P_3 of model (1) is globally asymptotically stable in Ω.*

Proof Consider a both-strain IEP $P_3 = (S^*, V^*, E^*_1, E^*_2, I^*_1, I^*_2, R^*)$, where S^*, V^*, E^*_1, E^*_2, I^*_1, I^*_2, R^* satisfy the following relations:

$$\varphi S^* = (1-a)\beta_1 V^* I^*_1 + \beta_2 V^* I^*_2 + \mu V^*, \tag{23}$$

$$\Lambda = \mu S^* + \mu V^* + (1-a)\beta_1 V^* I^*_1 + A\beta_1 S^* I^*_1 + \beta_2 V^* I^*_2 + A\beta_2 S^* I^*_2, \tag{24}$$

$$(\mu+\alpha_1)E^*_1 = (1-a)\beta_1 V^* I^*_1 + A\beta_1 S^* I^*_1, \tag{25}$$

$$(\mu+\alpha_2)E^*_1 = \beta_2 V^* I^*_1 + A\beta_2 S^* I^*_2, \tag{26}$$

$$(\mu+\alpha_1)(\gamma_1+\mu_1+\mu) = \alpha_1(1-a)\beta_1 V^* + A\alpha_1\beta_1 S^*, \tag{27}$$

$$(\mu+\alpha_2)(\gamma_2+\mu_2+\mu) = \alpha_2\beta_2 V^* + A\alpha_2\beta_2 S^*. \tag{28}$$

In order to prove the global asymptotic stability of the endemic equilibrium point P_3, Consider the following Lyapunov function:

$$\begin{aligned}W_2 = \;& S - S^* - S^*\ln\frac{S}{S^*} + V - V^* - V^*\ln\frac{V}{V^*} + E_1 - E^*_1 - E^*_1\ln\frac{E_1}{E^*_1} + E_2 - E^*_2 - E^*_2\ln\frac{E_2}{E^*_2}\\ &+\frac{\alpha_1+\mu}{\alpha_1}\left[I_1 - I^*_1 - I^*_1\ln\frac{I_1}{I^*_1}\right] + \frac{\alpha_2+\mu}{\alpha_2}\left[I_2 - I^*_2 - I^*_2\ln\frac{I_2}{I^*_2}\right].\end{aligned}$$

The time-derivative of W_2, along solutions of model (1) is given by

$$\begin{aligned}\dot{W}_2 &= \left(1-\frac{S^*}{S}\right)\dot{S}+\left(1-\frac{V^*}{V}\right)\dot{V}+\left(1-\frac{E_1^*}{E_1}\right)\dot{E}_1+\left(1-\frac{E_2^*}{E_2}\right)\dot{E}_2+\frac{\alpha_1+\mu}{\alpha_1}\left(1-\frac{I_1^*}{I_1}\right)\dot{I}_1+\frac{\alpha_2+\mu}{\alpha_2}\left(1-\frac{I_2^*}{I_2}\right)\dot{I}_2\\ &= \left(1-\frac{S^*}{S}\right)[\Lambda-A\beta_1SI_1-A\beta_2SI_2-(\varphi+\mu)S]+\left(1-\frac{V^*}{V}\right)[\varphi S-(1-a)\beta_1VI_1-\beta_2VI_2-\mu V]\\ &\quad+\left(1-\frac{E_1^*}{E_1}\right)[A\beta_1SI_1+(1-a)\beta_1VI_1-(\alpha_1+\mu)E_1]+\left(1-\frac{E_2^*}{E_2}\right)[A\beta_2SI_2+\beta_2VI_2-(\alpha_2+\mu)E_2]\\ &\quad+\frac{\alpha_1+\mu}{\alpha_1}\left(1-\frac{I_1^*}{I_1}\right)[\alpha_1E_1-(\gamma_1+\mu_1+\mu)I_1]+\frac{\alpha_2+\mu}{\alpha_2}\left(1-\frac{I_2^*}{I_2}\right)[\alpha_2E_2-(\gamma_2+\mu_2+\mu)I_2].\end{aligned}$$

Together with (23)–(28), we have

$$\begin{aligned}\dot{W}_2 &= \mu S^*\left(2-\frac{S}{S^*}-\frac{S^*}{S}\right)+\mu V^*\left(3-\frac{S^*}{S}-\frac{V}{V^*}-\frac{S}{S^*}\frac{V^*}{V}\right)\\ &\quad+A\beta_1S^*I_1^*\left(3-\frac{S^*}{S}-\frac{I_1}{I_1^*}\frac{S}{S^*}\frac{E_1^*}{E_1}-\frac{E_1}{E_1^*}\frac{I_1^*}{I_1}\right)\\ &\quad+A\beta_2S^*I_2^*\left(3-\frac{S^*}{S}-\frac{I_2}{I_2^*}\frac{S}{S^*}\frac{E_2^*}{E_2}-\frac{E_2}{E_2^*}\frac{I_2^*}{I_2}\right)\\ &\quad+(1-a)\beta_1V^*I_1^*\left(4-\frac{S}{S^*}\frac{V^*}{V}-\frac{I_1}{I_1^*}\frac{V}{V^*}\frac{E_1^*}{E_1}-\frac{E_1}{E_1^*}\frac{I_1^*}{I_1}-\frac{S^*}{S}\right)\\ &\quad+\beta_2V^*I_2^*\left(4-\frac{S}{S^*}\frac{V^*}{V}-\frac{I_2}{I_2^*}\frac{V}{V^*}\frac{E_2^*}{E_2}-\frac{E_2}{E_2^*}\frac{I_2^*}{I_2}-\frac{S^*}{S}\right).\end{aligned}$$

Then the proof follows the same approach and steps as in the above Theorem 3.6. Further, it can be proved that $M_2=\{P_3\}$ is the largest compact invariant subset of $\left\{(S,V,E_1,E_2,I_1,I_2,R)\in\Omega:\dot{W}_2=0\right\}$. Consequently, by LaSalle's invariance principle, the endemic equilibrium point P_3 of model (1) is globally asymptotically stable. □

Theorem 3.8. *Let $\mathcal{R}_0^2>\mathcal{R}_0^1>1$. Then the second strain is dominant and the first strain is excluded. That is, any positive solution of model (1) satisfies*

$$(S(t),V(t),E_1(t),E_2(t),I_1(t),I_2(t))\to(S_{SS}^*,V_{SS}^*,0,E_2^*,0,I_2^*)\quad as\quad t\to\infty.$$

Proof First, from the third and fourth equations of (10), we notice that

$$\frac{(\gamma_1+\mu_1+\mu)(\alpha_1+\mu)}{\alpha_1}=A\beta_1S_{FS}^*+(1-a)\beta_1V_{FS}^*.$$

Then we note that the basic reproduction number can be rewritten as

$$\frac{1}{\mathcal{R}_0^1}=[AS_{FS}^*+(1-a)V_{FS}^*]\frac{\mu(\varphi+\mu)}{\Lambda[A\mu+(1-a)\varphi]},$$

and the basic reproduction number of the second strain follows the same approach and steps as

$$\frac{1}{\mathcal{R}_0^2}=[AS_{SS}^*+V_{SS}^*]\frac{\mu(\varphi+\mu)}{\Lambda[A\mu+\varphi]}.$$

Thus, $\mathcal{R}_0^2>\mathcal{R}_0^1>1$ implies that

$$\frac{AS_{FS}^{*}+(1-a)V_{FS}^{*}}{A\mu+(1-a)\varphi}>\frac{AS_{SS}^{*}+V_{SS}^{*}}{A\mu+\varphi}.$$
$$\frac{AS_{FS}^{*}+(1-a)V_{FS}^{*}}{A\mu+(1-a)\varphi}>\frac{AS_{SS}^{*}+(1-a)V_{SS}^{*}}{A\mu+\varphi}. \tag{29}$$

Set

$$z_1=\frac{1}{A\mu+\varphi}, z_2=\frac{\mu+\alpha_1}{\alpha_1[A\mu+(1-a)\varphi]}. \tag{30}$$

Now, let us consider the Lyapunov function:

$$\begin{aligned} W_3 &= S-S_{SS}^{*}-S_{SS}^{*}\ln\frac{S}{S_{SS}^{*}}+V-V_{SS}^{*}-V_{SS}^{*}\ln\frac{V}{V_{SS}^{*}}+E_2-E_2^{*}-E_2^{*}\ln\frac{E_2}{E_2^{*}}\\ &\quad+\frac{\alpha_2+\mu}{\alpha_2}\left(I_2-I_2^{*}-I_2^{*}\ln\frac{I_2}{I_2^{*}}\right)+z_1E_1+z_2I_1. \end{aligned}$$

Calculating the derivative of W_3 along the solution of (1), we obtain

$$\begin{aligned} \dot{W}_3 &= \left(1-\frac{S_{SS}^{*}}{S}\right)\dot{S}+\left(1-\frac{V_{SS}^{*}}{V}\right)\dot{V}+\left(1-\frac{E_2^{*}}{E_2}\right)\dot{E}_2+\frac{\alpha_2+\mu}{\alpha_2}\left(1-\frac{I_2^{*}}{I_2}\right)\dot{I}_2+z_1E_1+z_2I_1\\ &= \left(1-\frac{S_{SS}^{*}}{S}\right)[\Lambda-A\beta_2SI_2-(\varphi+\mu)S]+\left(1-\frac{V_{SS}^{*}}{V}\right)[\varphi S-(1-a)\beta_2VI_2-\mu V]\\ &\quad+\left(1-\frac{E_2^{*}}{E_2}\right)[A\beta_2SI_2+\beta_2VI_2-(\alpha_2+\mu)E_2]\\ &\quad+\frac{\alpha_2+\mu}{\alpha_2}\left(1-\frac{I_2^{*}}{I_2}\right)[\alpha_2E_2-(\gamma_2+\mu_2+\mu)I_2]+z_1E_1+z_2I_1\\ &= \mu S_{SS}^{*}\left(2-\frac{S}{S_{SS}^{*}}-\frac{S_{SS}^{*}}{S}\right)+\mu V_{SS}^{*}\left(3-\frac{S_{SS}^{*}}{S}-\frac{V}{V_{SS}^{*}}-\frac{S}{S_{SS}^{*}}\frac{V_{SS}^{*}}{V}\right)\\ &\quad+A\beta_2S_{SS}^{*}I_2^{*}\left(3-\frac{S_{SS}^{*}}{S}-\frac{I_2}{I_2^{*}}\frac{S}{S_{SS}^{*}}\frac{E_2^{*}}{E_2}-\frac{E_2}{E_2^{*}}\frac{I_2^{*}}{I_2}\right)\\ &\quad+(1-a)\beta_2V_{SS}^{*}I_2^{*}\left(4-\frac{S}{S_{SS}^{*}}\frac{V_{SS}^{*}}{V}-\frac{I_2}{I_2^{*}}\frac{V}{V_{SS}^{*}}\frac{E_2^{*}}{E_2}-\frac{E_2}{E_2^{*}}\frac{I_2^{*}}{I_2}-\frac{S_{SS}^{*}}{S}\right)\\ &\quad+\frac{A\beta_1S_{SS}^{*}I_1+(1-a)\beta_1V_{SS}^{*}I_1}{A\mu+\varphi}+\frac{(\mu+\alpha_1)E_1}{A\mu+\varphi}-\frac{(\mu+\alpha_1)E_1}{A\mu+(1-a)\varphi}\\ &\quad-\frac{A\beta_1S_{FS}^{*}I_1+(1-a)\beta_1V_{FS}^{*}I_1}{A\mu+(1-a)\varphi}\\ &= \mu S_{SS}^{*}\left(2-\frac{S}{S_{SS}^{*}}-\frac{S_{SS}^{*}}{S}\right)+\mu V_{SS}^{*}\left(3-\frac{S_{SS}^{*}}{S}-\frac{V}{V_{SS}^{*}}-\frac{S}{S_{SS}^{*}}\frac{V_{SS}^{*}}{V}\right)\\ &\quad+A\beta_2S_{SS}^{*}I_2^{*}\left(3-\frac{S_{SS}^{*}}{S}-\frac{I_2}{I_2^{*}}\frac{S}{S_{SS}^{*}}\frac{E_2^{*}}{E_2}-\frac{E_2}{E_2^{*}}\frac{I_2^{*}}{I_2}\right)\\ &\quad+(1-a)\beta_2V_{SS}^{*}I_2^{*}\left(4-\frac{S}{S_{SS}^{*}}\frac{V_{SS}^{*}}{V}-\frac{I_2}{I_2^{*}}\frac{V}{V_{SS}^{*}}\frac{E_2^{*}}{E_2}-\frac{E_2}{E_2^{*}}\frac{I_2^{*}}{I_2}-\frac{S_{SS}^{*}}{S}\right)\\ &\quad+\beta_1I_1\left(\frac{AS_{SS}^{*}+(1-a)V_{SS}^{*}}{A\mu+\varphi}-\frac{AS_{FS}^{*}+(1-a)V_{FS}^{*}}{A\mu+(1-a)\varphi}\right)-\frac{a\varphi(\mu+\alpha_2)E_1}{[A\mu+\varphi][A\mu+(1-a)\varphi]}. \end{aligned}$$

Let

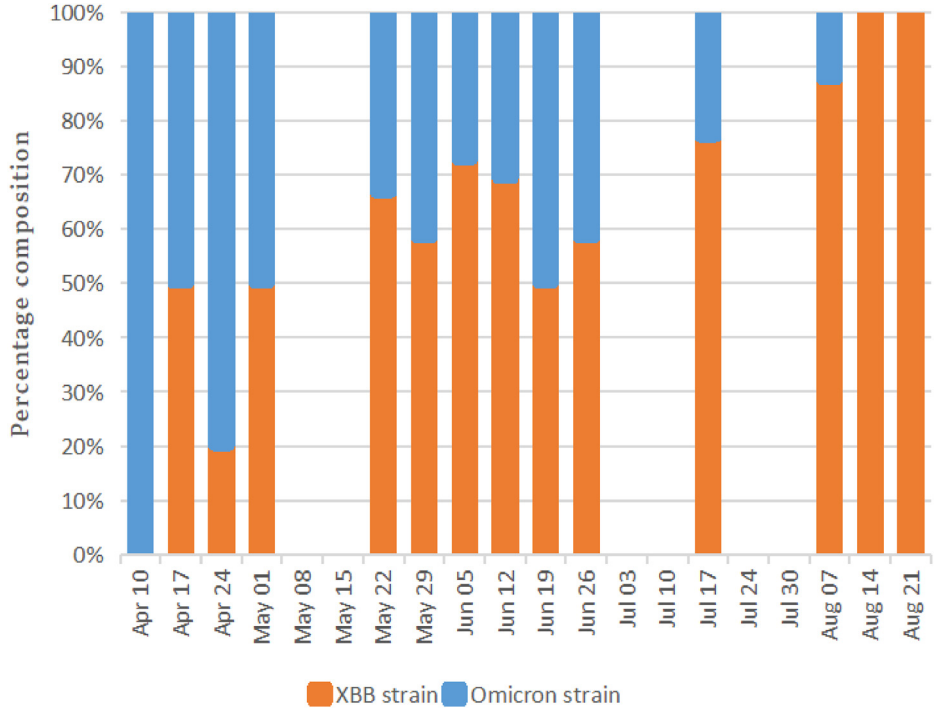

Fig. 2. Percentage composition of Omicron strain and XBB strain for Jinzhou COVID-19 epidemic in 2023.

$$\Omega = \left\{(S, V, E_1, E_2, I_1, I_2) \in \mathbb{R}^4_+ \times \mathbb{R}^2_+ : \dot{W}_3 = 0\right\}.$$

Since $\mathcal{R}_0^2 > \mathcal{R}_0^1 > 1$, by (29) we see that a solution of (1) in Ω for all t exhibits $I_1(t) \equiv E_1(t) = 0$. We conclude the maximal compact invariant set in Ω satisfies

$$S = S^*_{SS}, \quad V = V^*_{SS}, \quad E_2 = E^*_2, \quad I_2 = I^*_2, \quad E_1 = 0, \quad I_1 = 0. \tag{31}$$

Therefore, the Lyapunov-LaSalle theorem in (Wang, 2022) implies that $(S^*_{SS}, V^*_{SS}, 0, E^*_2, 0, I^*_2)$ is globally stable. This proves the theorem. □

4. Data fitting and numerical simulations

4.1. Two-strain data and analysis

The two-strain surveillance data and the weekly percentages of XBB cases, for Jinzhou COVID-19 epidemic (April 10, 2023—September 17, 2023), were provided by Jinzhou Center for Disease Control and Prevention (i.e., Jinzhou CDC) in this study. In detail, the XBB strain in orange dominated and replaced the Omicron strain in blue within two months in Fig. 2, the specific percentages of XBB cases were collected in Table 1. The daily percentage of XBB strain in orange was estimated in Fig. 3 using the cubic spline interpolation and the surveillance data. Combined the surveillance data and the percentages of two strains, daily numbers of Omicron cases and XBB cases were obtained from 10 April to 29 September of 2023 in Fig. 4. Further, the transmission evolution for Omicron strain and XBB strain were reflected within the total population.

4.2. Data fitting with parameter estimation

The infection cases being detected between April 10 and September 17 caused by either Omicron strain or XBB strain, as reported by Jinzhou CDC. The percentage of the susceptible who had protection awareness was 50%, and they could reduce their infection rate by 50% through control measures such as increasing their social distance and wearing masks. By using of least squares method, the specific percentages in Fig. 4 and the parameter values in Table 2, the fitting curves for Jinzhou COVID-19 epidemic were performed with 6434 infection cases and 9 deaths as of September 17, 2023 in Fig. 5, of which 1711 infected cases with Omicron strain in yellow and 4723 infected cases with XBB strain in red were respectively derived. Then,

Table 1
Weekly percentage of XBB strain for Jinzhou COVID-19 epidemic in 2023.

No.	Date	Percentage(%)	No.	Date	Percentage(%)	No.	Date	Percentage(%)
1	Apr 10	00.00	6	May 29	58.33	11	Jul 17	76.92
2	Apr 17	50.00	7	Jun 05	72.73	12	Aug 07	87.50
3	Apr 24	20.00	8	Jun 12	69.23	13	Aug 14	100.00
4	May 01	50.00	9	Jun 19	50.00	14	Aug 21	100.00
5	May 22	66.67	10	Jun 26	58.33			

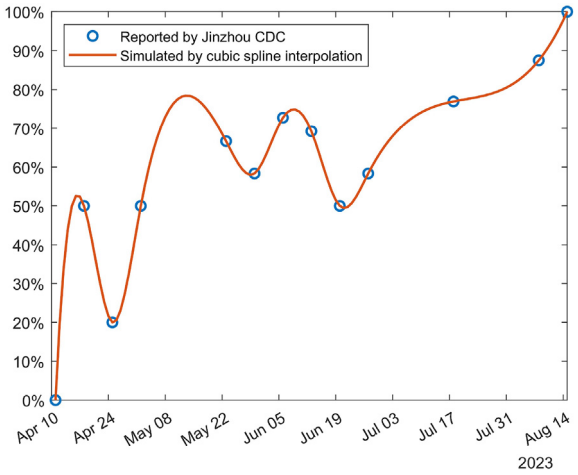

Fig. 3. Daily percentage of XBB strain using cubic spline interpolation and the surveillance data from Jinzhou CDC.

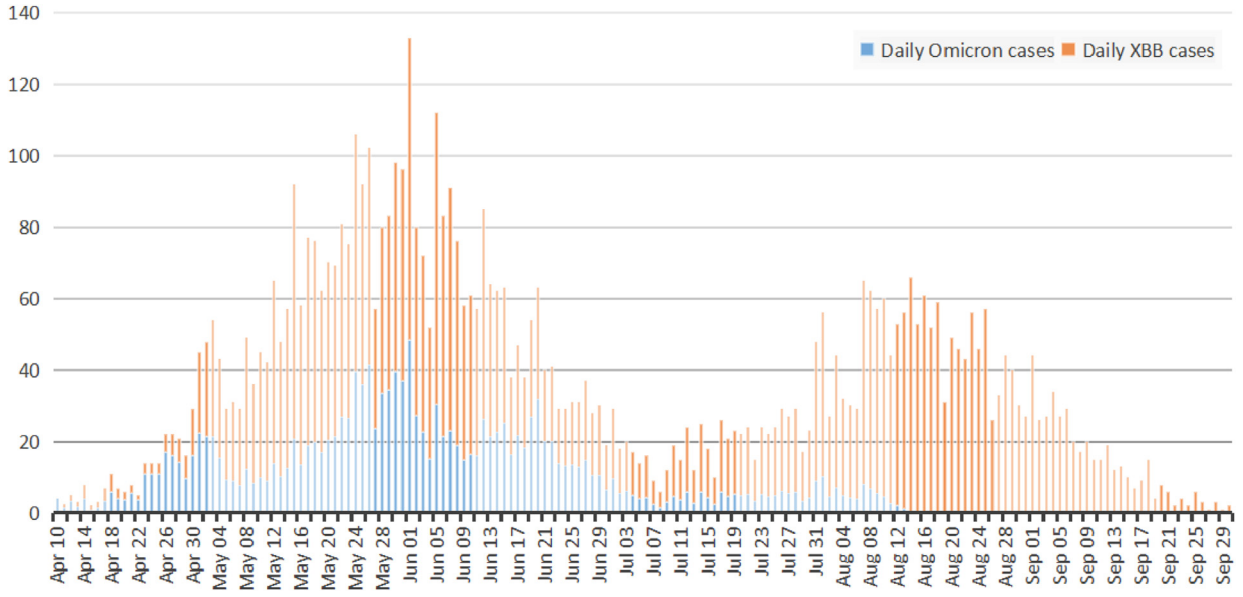

Fig. 4. Daily cases of Omicron strain and XBB strain for Jinzhou COVID-19 epidemic in 2023 using cubic spline interpolation.

the relationship between the basic reproduction number $\mathcal{R}_0$ and the parameters (i.e., q, g) of protection awareness is investigated in Fig. 6. If q and g are set to 0.9 and 0.1 respectively, the basic reproduction number is 1.61. If q and g are set to 0.1 and 0.9 respectively, the basic reproduction number is 0.30.

Table 2
Parameter values for Jinzhou COVID-19 epidemic in 2023.

Parameter	Value	Source	Parameter	Value	Source
Λ	190.0	Jinzhou Bureau of Statistics (2016)	a	0.8700	(Fu et al., 2023; Li, Song, et al., 2022; Pilishvili et al., 2021; Tchoumi et al., 2022; Thompson et al., 2021; Zou, Huang, et al., 2022)
β_1	1.4689×10^{-7}	Fitted	α_1	0.2500	Fitted
β_2	2.7610×10^{-7}	Fitted	α_2	0.4000	Fitted
q	0.5000	Fitted	μ_1	0.0030	Guo and Li (2023)
g	0.5000	Fitted	μ_2	0.0009	Fitted
φ	0.0024	National Health Commission of Jinzhou (2021)	γ_1	0.1429	Fitted
μ	2.5600×10^{-9}	Jinzhou Bureau of Statistics (2016)	γ_2	0.3333	Fitted

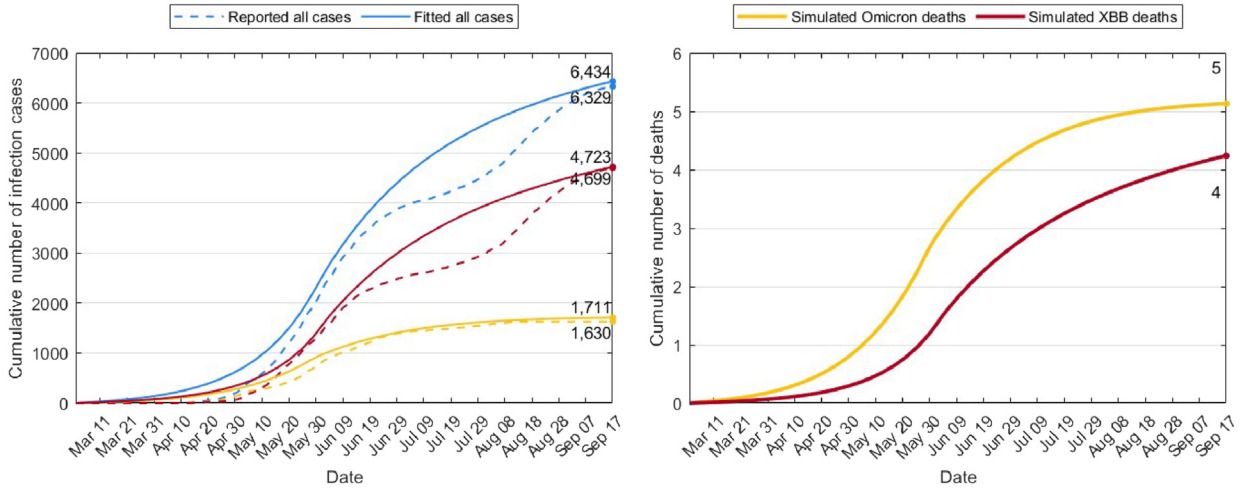

Fig. 5. Data fittings of Jinzhou COVID-19 epidemic (Left). Simulated deaths for Omicron strain and XBB strain as of September 17, 2023 (Right).

4.3. Sensitivity analysis

The global sensitivity analysis using the Latin Hypercube Sampling (LHS) and Partial Rank Correlation Coefficients (PRCCs) was performed to investigate the relationship between the parameters and the peak number of the infected of two-stain SVEIR model, when the sample size was set to be 1000 and the p-value was set less than 0.01 in Fig. 7. The values of PRCCs and their significance for all parameters on the peak number of the infected were shown in Table 3. Nine parameters with stars played the key role on the peak number of the infected in Fig. 7. Especially, β_2, α_2, γ_2 associated with XBB strain took the greater effects than β_1, α_1, γ_1 for Omicron strain, which reflected the greater infectivity of XBB strain. Meanwhile, the parameters q and g associated with protection awareness of the susceptible had significant role for the control of the virus spread.

5. Discussion

5.1. Investigation on transmission scenario

If the infection rates of two strains were increased by 50%, then the infection scales would be increased rapidly in Fig. 8. As of September 17, the infection scales caused by XBB strain and Omicron strain were increased from baseline to 1,028,697 and 39,170, respectively. The corresponding deaths increased to 926 cases and 118 cases. If the mean incubation periods of two strains were decreased by 50%, then the infection scales would be tripled in Fig. 8. As of September 17, the infection scales of two strains were increased to 15,221 and 4289, respectively, and deaths were increased slightly, to 27 cases. Therefore, the future strain with the larger infection rate or the smaller incubation period would cause the larger infection scale. Especially, one infection rate increased, the risks of reseiving deaths enhanced a lot.

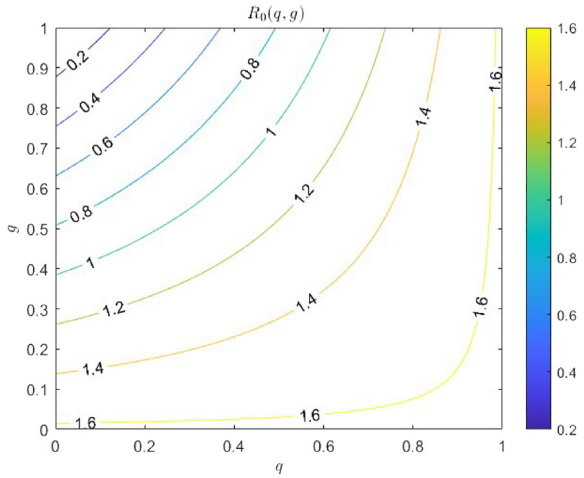

Fig. 6. Contour plot of sensitivity of $\mathcal{R}_0(q,g)$.

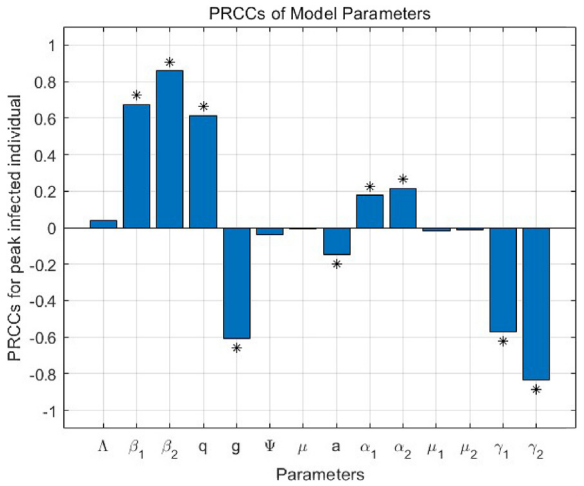

Fig. 7. The values of PRCCs and significance for the peak number of the infected to two-strain SVEIR model. (*) denoted that the PRCCs were significant.

Table 3
PRCCs values for the peak number of infected.

Parameter	PRCC	P-value	Parameter	PRCC	P-value
Λ	0.0382	0.2300	a	−0.1474	0.0000
β_1	0.6752	0.0000	α_1	0.1758	0.0000
β_2	0.8575	0.0000	α_2	0.2140	0.0000
q	0.6142	0.0000	μ_1	−0.0180	0.5712
g	−0.6066	0.0000	μ_2	−0.0133	0.6768
φ	−0.0397	0.2125	γ_1	−0.5725	0.0000
μ	0.0090	0.7772	γ_2	−0.8350	0.0000

5.2. Investigation on protection awareness

The percentage of susceptible without protection awareness and the protection efficiency against the infection scales of two strains were investigated. The results showed that, as of September 17, the infection scales with Omicron strain increased from 930 to 3186, the infection scales with XBB strain varied from 1534 to 15,181, as percentage of susceptible without protection awareness increased from 0.4 to 0.6 in the first two graphs in Fig. 9. Let the protection efficiency be 0.3, 0.5, 0.7, the infection scales for both strains dropped to hundreds of infection cases with the increasing of protection efficiency. So, the enhancement of percentage of susceptible with protection awareness or the protection efficiency surppressed the infection

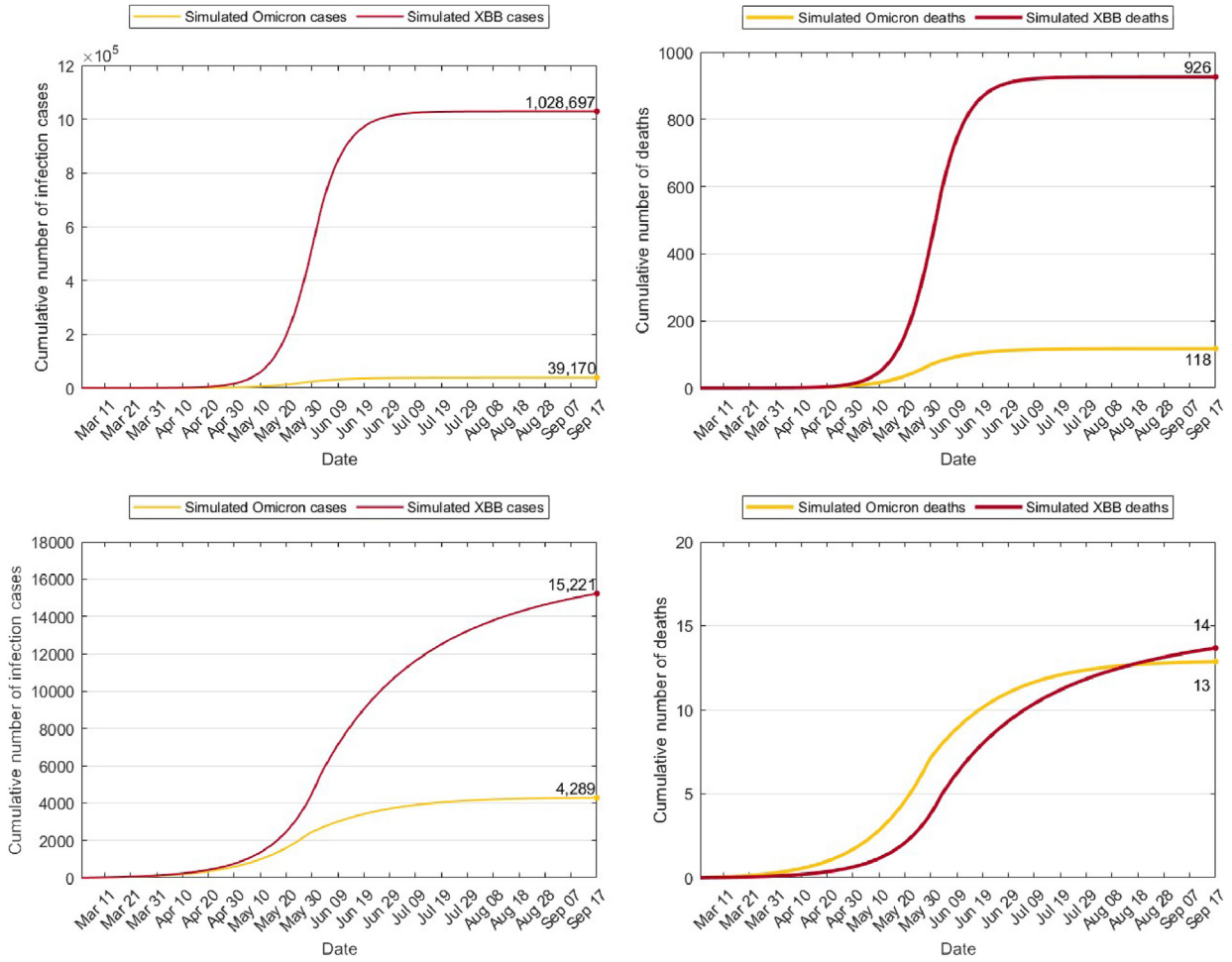

Fig. 8. Simulation scales of infection cases (Left) and deaths (Right) by two-strain SVEIR model. $1.5\beta_1$, $1.5\beta_2$ (Top) and $0.5\alpha_1$, $0.5\alpha_2$ (Bottom).

scales and deaths for the future strain. Moreover, the infection scale with positive combination control strategy for Omicron strain declined from 1711 to 236, and for XBB strain decreased from 4723 to 154; while the infection scales with negative combination strategy significantly increase for two stains in Fig. 9. Compared with the surveillance data, the saved infection scales at least reach 1556 and 10,482 in Table 4. Further, the time that the public who produce protection awareness is explored against the infection scale. If April 10 is set as the date for baseline, and protection awareness of the public is produced on May 20, as of September 17, then the infection scale with Omicron strain increases from 1711 to 16,008, the infection scales with XBB strain varies from 4723 to 160,062 in the top of Fig. 10. If protection efficiency varies with the time, then the infection scales of two strains decrease in the bottom of Fig. 10.

5.3. Investigation on two-strain SVEIR model

In this study, two-strain SVEIR model describes the transmission mechanism of COVID-19, which is more consistent with the real situation by introducing the exposed within the total population, compared to the model by Tchoumi et al. (Tchoumi et al., 2022). The results of two-strain SVEIR model show that the incubation period of the exposed impacts on the infection scale of the epidemic. Compared to Wang's model in (Wang, 2022), the effect of vaccination is considered in two-strain SVEIR model, because vaccine acts as the primary method of prevention and control after the closure of the dynamic zero-COVID policy. Compared to Vashishth and Basaiti's model in (Vashishth & Basaiti, 2024), the protection awareness of the susceptible is concerned, and the effect of protection awareness on the infection scale is then explored. As the consequences, the results of this study show that, except for vaccination campaigns and non-pharmacological interventions, the time that the public who produce protection awareness and the protection efficiency are also vital to the variations of infection scales.

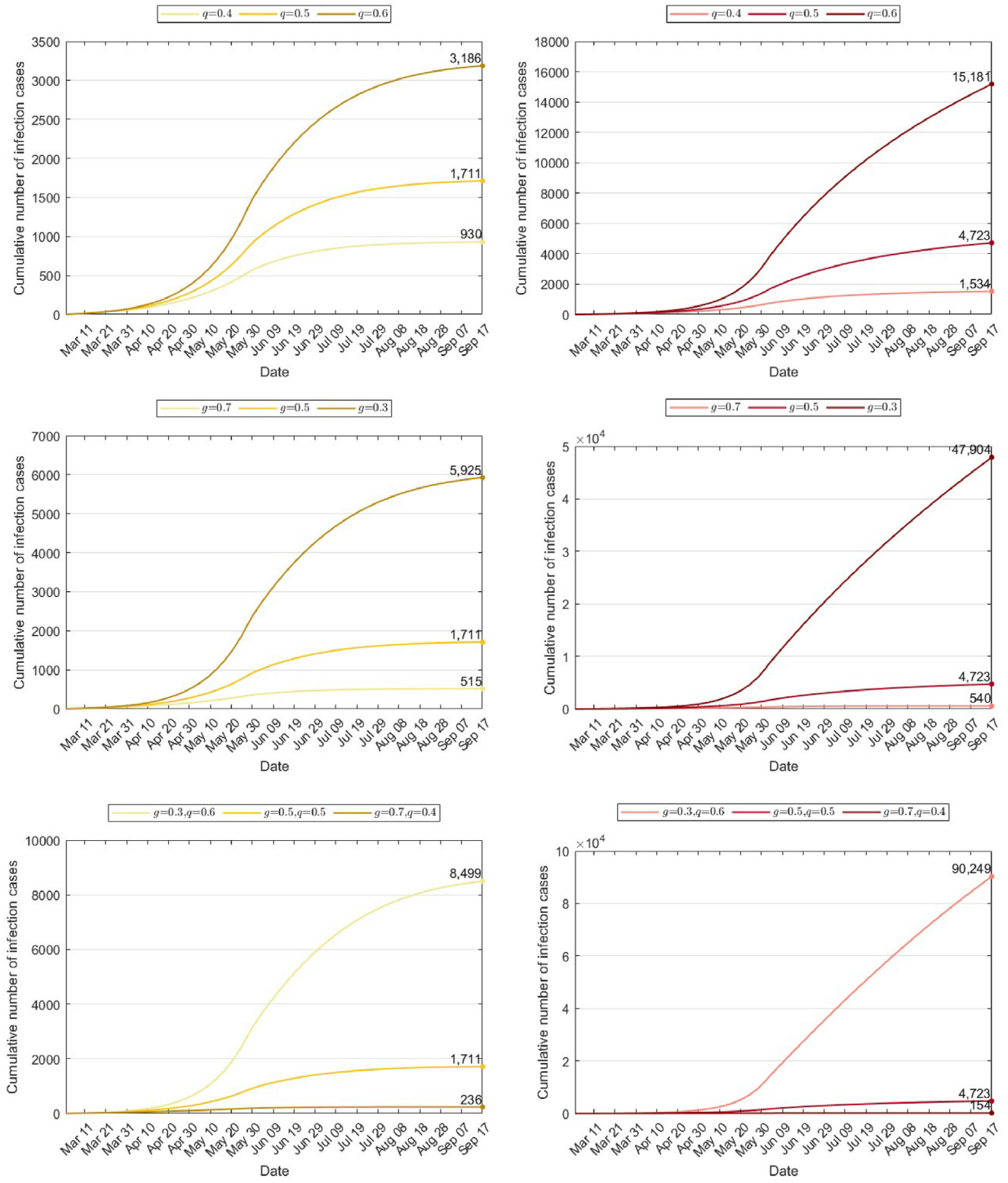

Fig. 9. Infection scales caused by Omicron strain (Left) and infection scales caused by XBB strain (Right) for four-type control strategies.

6. Conclusion

In this study, a two-strain SVEIR model with protection awareness is developed. The first consideration is that the expression for the basic reproduction number was calculated using the next generation matrix method. The disease-free equilibrium point of the two-strain SVEIR model is proved to be locally asymptotically stable and globally asymptotically

Table 4
Infection scales of Jinzhou COVID-19 epidemic with four strategies in 2023.

Strategy	Impact	q	g	Omicron-strain			XBB-strain		
				Fitted[a]	Saved[b]	Will save[c]	Fitted	Saved	Will save
Baseline control	–	0.5	0.5	1711	–	–	4723	–	–
Separate control (q)	Negative	0.6	0.5	3186[d]	1556	–	15,181	10,482	–
	Positive	0.4	0.5	930	–	700	1534	–	3165
Separate control (g)	Negative	0.5	0.3	5925	4295	–	47,904	43,205	–
	Positive	0.5	0.7	515	–	1115	540	–	4159
Combination control (q and g)	Negative	0.6	0.3	8499	6869	–	90,249	85,550	–
	Positive	0.4	0.7	236	–	1394	154	–	4545

[a] Fitted is referred as infections by SVEIR model. [b] Saved is meant for the difference between simulated infection and surveillance data. [c] Will saved is denoted by the difference between surveillance data and simulated infection. [d] As of September 17, the surveillance data for Omicron strain is 1630, and the surveillance data for XBB strain is 4699. $1556 = 3186 - 1630$.

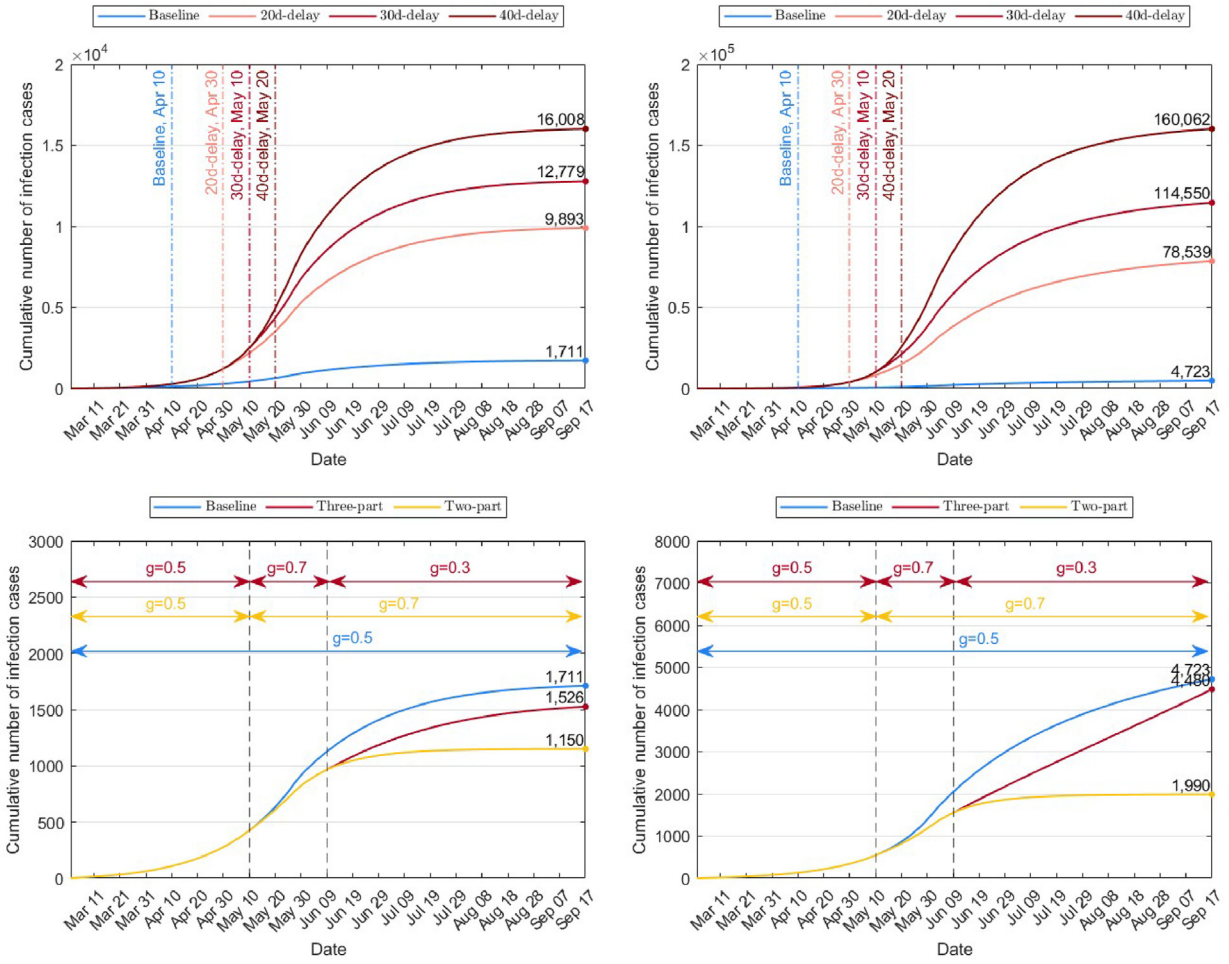

Fig. 10. Infection scales caused by Omicron strain (Left) and infection scales caused by XBB strain (Right). The time that the public who produce protection awareness is shifted away 20 days, 30 days and 40 days from April 10 with baseline (Top). The protection efficiency varies with three-part phase, two-part phase and baseline phase (Bottom).

stable when $\mathcal{R}_0 < 1$ was valid. Then the SVEIR model admits an infection equilibrium point for first-strain when $\mathcal{R}_0^1 > 1$ held, and also has an infection equlibrium point for second-strain when $\mathcal{R}_0^2 > 1$ holds. Meanwhile, when $\mathcal{R}_0^1 > 1$ and $\mathcal{R}_0^2 > 1$ hold, there exists an interior equilibrium point when both strains are prevalent simultaneously. Further, the global asymptotic stability of the interior equilibrium point is proved using Lyapunov function and LaSalle's invariance principle. In addition, the Lyapunov-LaSalle theorem is also used to show the property of competitive exclusion of the SVEIR model with one dominant strain.

The interactions of the virus transmission against human behaviors are explored by analyzing the impacts of protection awareness among the population of Jinzhou City. Using the percentages of both strains in Fig. 2 and daily infections of Jinzhou COVID-19 epidemic from 10 April to 17 September of 2023, the two-strain SVEIR model is used to fit the tendencies of Omicron strain and XBB strain. The infection scale of XBB strain gradually exceeds and dominates in the transmission, the competitive exclusion relationship for both strains of Jinzhou COVID-19 epidemic within five months occurred in Fig. 4. Data fittings and parameter estimations are performed by least squares mathed in Fig. 5. The simulation result shows that the percentage of the susceptible without protection awareness is positively correlated with the basic reproduction number (i.e., $\mathcal{R}_0$), and that the enhancement of the protection efficiency of the susceptible leads to the reduction of the basic reproduction number (i.e., $\mathcal{R}_0$) in Fig. 6. Meanwhile, using the PRCC global sensitivity analysis, the parameters associated with XBB strain presents the greater impacts on the peak of the infected, compared to those with Omicron strain in Fig. 7, and the parameters associated with protection awareness also played an significant role on the peak of the infected. If the infection rates are increased by 50%, then the infection and death scales will increase significantly. If the incubation periods are decreased by 50%, then the similar tendency is presented in Fig. 8. If the protection awareness campaigns are strengthened and self-protection measures of the individuals were increased, then the infection scales will be effectively controlled, which are supported by the numerical simulations in Fig. 9. Especially, if the time that the public who produce protection awareness become earlier, or, if protection efficiency varies with time during the epidemic, then the infection scales of two strains will decrease, as illustrated by the results in Fig. 10. To control the infection scale, according to the current situation of medical sources in the given region, we recommend that the officials from public health agents to promote the establishments of the self-protection measures such as wearing masks, increasing social distance and prompt self-disinfection.

CRediT authorship contribution statement

Kaijing Chen: Writing – review & editing, Writing – original draft, Visualization, Validation, Software, Methodology, Investigation, Formal analysis, Conceptualization. **Fengying Wei:** Writing – review & editing, Supervision, Resources, Project administration, Methodology, Formal analysis. **Xinyan Zhang:** Project administration, Funding acquisition, Data curation. **Hao Jin:** Data curation. **Ruiyang Zhou:** Software. **Yue Zuo:** Data curation. **Kai Fan:** Data curation.

Ethics approval and consent to participate

The ethical approval and individual consents were exempted as the aggregated data were used in this study.

Data and material availability

The data that supported this article may be available upon reasonable request to the corresponding author.

Funding

This study received was supported by the Natural Science Foundation of Fujian Province of China (2021J01621), Special Projects of the Central Government Guiding Local Science and Technology Development (2021L3018), Consultancy Project by the Chinese Academy of Engineering (2022-JB-06, 2023-JB-12), Project for epidemiological characteristics analysis and clustering epidemics analysis of COVID-19 in Jinzhou City (JZ2024B066).

Declaration of competing interest

All authors declared that we did not and do not have any conflicts of interest with any other institutions and groups.

We all read and agreed to submit the manuscript entitled Dynamics of an SVEIR transmis-sion model with protection awareness and two strains to an international high-quality journal Infectious Disease Modelling for academic communications with other researchers in the field of infectious diseases and their dynamics around the world.

Acknowledgements

We thank Prof. Bo Deng for his good and valuable comments. This study received the supports from Natural Science Foundation of Fujian Province of China (2021J01621), Special Projects of the Central Government Guiding Local Science and Technology Development (2021L3018), Consultancy Project by the Chinese Academy of Engineering (2022-JB-06, 2023-JB-12), Project for epidemiological characteristics analysis and clustering epidemics analysis of COVID-19 in Jinzhou City (JZ2024B066).

References

Andrews, N., Tessier, E., Stowe, J., Gower, C., Kirsebom, F., Simmons, R., et al. (2022). Duration of protection against mild and severe disease by Covid-19 vaccines. *New England Journal of Medicine, 386*, 340–350. https://doi.org/10.1056/NEJMoa2115481

Arruda, E. F., Das, S. S., Dias, C. M., & Pastore, D. H. (2021). Modelling and optimal control of multi strain epidemics, with application to COVID-19. *PLoS One, 16*, Article e257512. https://doi.org/10.1371/journal.pone.0257512
Chen, K., Wei, F., Zhang, X., Jin, H., Wang, Z., Zuo, Y., et al. (2024). Epidemiological feature analysis of SVEIR model with control strategy and variant evolution. *Infectious Disease Modelling, 9*, 689–700. https://doi.org/10.1016/j.idm.2024.03.005
Collinson, S., & Heffernan, J. M. (2014). Modelling the effects of media during an influenza epidemic. Collinson and Heffernan. *BMC Public Health, 14*, 376. https://doi.org/10.1186/1471-2458-14-376
Cui, T., & Liu, P. (2022). Fractional transmission analysis of two strains of influenza dynamics. *Results in Physics, 40*, Article 105843. https://doi.org/10.1016/j.rinp.2022.105843
Cui, J., Sun, Y., & Zhu, H. (2008). The impact of media on the control of infectious diseases. *Journal of Dynamics and Differential Equations, 20*, 31–53. https://doi.org/10.1007/s10884-007-9075-0
de Leon, U. A., Avila-Vales, E., & Huang, K. (2022). Modeling COVID-19 dynamic using a two-strain model with vaccination. *Chaos, Solitons & Fractals, 157*, Article 111927. https://doi.org/10.1016/j.chaos.2022.111927
Fu, D., He, G., Li, H., Tan, H., Ji, X., Lin, Z., et al. (2023). Effectiveness of COVID-19 vaccination against SARS-CoV-2 Omicron variant infection and symptoms-China, December 2022-February 2023. *China CDC Weekly, 5*, 369–373. https://doi.org/10.46234/ccdcw2023.070
Gao, S., Shen, M., Wang, X., Wang, J., Martcheva, M., & Rong, L. (2023). A multi-strain model with asymptomatic transmission: Application to COVID-19 in the US. *Journal of Theoretical Biology, 565*, Article 111468. https://doi.org/10.1016/j.jtbi.2023.111468
Garcia-Beltran, W. F., St Denis, K. J., Hoelzemer, A., Lam, E. C., Nitido, A. D., Sheehan, M. L., et al. (2022). mRNA-based COVID-19 vaccine boosters induce neutralizing immunity against SARS-CoV-2 Omicron variant. *Cell, 185*, 457–466. https://doi.org/10.1016/j.cell.2021.12.033
Gonzalez-Parra, G., Martínez-Rodríguez, D., & Villanueva-Micó, R. (2021). Impact of a new SARS-CoV-2 variant on the population: A mathematical modeling approach. *Mathematical and Computational Applications, 26*, 25. https://doi.org/10.3390/mca26020025
Guo, Y., & Li, T. (2023). Modeling the competitive transmission of the Omicron strain and Delta strain of COVID-19. *Journal of Mathematical Analysis and Applications, 526*, Article 127283. https://doi.org/10.1016/j.jmaa.2023.127283
Guo, Y., Ye, W., Zhao, Z., Guo, X., Song, W., Su, Y., et al. (2023). Simulating potential outbreaks of Delta and Omicron variants based on contact-tracing data: A modelling study in Fujian Province, China. *Infectious Disease Modelling, 8*, 270–281. https://doi.org/10.1016/j.idm.2023.02.002
Hall, V., Foulkes, S., Insalata, F., Kirwan, P., Saei, A., Atti, A., et al. (2022). Protection against SARS-CoV-2 after Covid-19 vaccination and previous infection. *New England Journal of Medicine, 386*, 1207–1220. https://doi.org/10.1056/NEJMoa2118691
Jinzhou Bureau of Statistics. (2016). Report on the demographic development of Jinzhou city. http://tjj.jz.gov.cn/info/1042/1850.htm.
Khatun, M. S., Das, S., & Das, P. (2023). Dynamics and control of an SITR COVID-19 model with awareness and hospital bed dependency. *Chaos, Solitons & Fractals, 175*, Article 114010. https://doi.org/10.1016/j.chaos.2023.114010
Kumar, R., Kumar, A., & Takeuchi, Y. (2019). Modeling the impact of sanitation and awareness on the spread of infectious diseases. *Mathematical Biosciences and Engineering, 16*, 667–700. https://doi.org/10.3934/mbe.2019032
Lan, X., Chen, G., Zhou, R., Zheng, K., Cai, S., Wei, F., et al. (2024). An SEIHR model with age group and social contact for analysis of Fuzhou COVID-19 large wave. *Infectious Disease Modelling, 9*, 728–743. https://doi.org/10.1016/j.idm.2024.04.003
Lauring, A. S., & Hodcroft, E. B. (2021). Genetic variants of SARS-CoV-2—what do they mean? *The Journal of the American Medical Association, 325*, 529–531. https://doi.org/10.1001/jama.2020.27124
Li, Y., & Cui, J. (2009). The effect of constant and pulse vaccination on SIS epidemic models incorporating media coverage. *Communications in Nonlinear Science and Numerical Simulation, 14*, 2353–2365. https://doi.org/10.1016/j.cnsns.2008.06.024
Li, J., Song, R., Yuan, Z., Xu, Z., Suo, L., Wang, Q., et al. (2022). Protective effect of inactivated COVID-19 vaccines against progression of SARS-CoV-2 Omicron and Delta variant infections to pneumonia in Beijing, China, in 2022. *Vaccines, 10*, 1215. https://doi.org/10.3390/vaccines10081215
Li, D., Wei, F., & Mao, X. (2022). Stationary distribution and density function of a stochastic SVIR epidemic model. *Journal of the Franklin Institute, 359*, 9422–9449. https://doi.org/10.1016/j.jfranklin.2022.09.026
Liu, C., Lu, J., Li, P., Feng, S., Guo, Y., Li, K., et al. (2023). A comparative study on epidemiological characteristics, transmissibility, and pathogenicity of three COVID-19 outbreaks caused by different variants. *International Journal of Infectious Diseases, 134*, 78–87. https://doi.org/10.1016/j.ijid.2023.01.039
Liu, F., & Wei, F. (2022). An epidemic model with Beddington-DeAngelis functional response and environmental fluctuations. *Physica A: Statistical Mechanics and Its Applications, 597*, Article 127321. https://doi.org/10.1016/j.physa.2022.127321
Liu, H., Xu, X., Deng, X., Hu, Z., Sun, R., et al. (2023). Counterfactual analysis of the 2023 Omicron XBB wave in China. *Infectious Disease Modelling, 9*, 195–203. https://doi.org/10.1016/j.idm.2023.12.006
Lu, R., & Wei, F. (2019). Persistence and extinction for an age-structured stochastic SVIR epidemic model with generalized nonlinear incidence rate. *Physica A: Statistical Mechanics and Its Applications, 513*, 572–587. https://doi.org/10.1016/j.physa.2018.09.016
National Health Commission of Jinzhou. (2021). Notice on further promotion of COVID-19 vaccination in the city. http://wjw.jz.gov.cn/info/1054/5327.htm.
Petrone, D., Mateo-Urdiales, A., Sacco, C., Riccardo, F., Bella, A., et al. (2023). Reduction of the risk of severe COVID-19 due to Omicron compared to Delta variant in Italy (November 2021-February 2022). *International Journal of Infectious Diseases, 129*, 135–141. https://doi.org/10.1016/j.ijid.2023.01.027
Pilishvili, T., Fleming-Dutra, K. E., Farrar, J. L., et al. (2021). Interim estimates of vaccine effectiveness of pfizer-BioNTech and moderna COVID-19 vaccines among health care personnel-33 U.S. sites, January-2021. *MMWR Morb Mortal Wkly Rep, 70*, 753–758. https://doi.org/10.15585/mmwr.mm7020e2
Shan, S., Luo, S., Yang, Z., Hong, J., Su, Y., Ding, F., et al. (2022). *Deep learning guided optimization of human antibody against SARS-CoV-2 variants with broad neutralization* (Vol. 119). Proceedings of the National Academy of Sciences. https://doi.org/10.1073/pnas.2122954119
Sun, Y., Wang, M., Wei, F., Huang, S., & Xu, J. (2023). COVID's future: Viral multi-lineage evolution and the dynamics of small epidemic waves without seasonality in COVID-19. *Journal of Biosafety and Biosecurity, 5*, 96–99. https://doi.org/10.1016/j.jobb.2023.07.003
Sun, C., Yang, W., Arino, J., & Khan, K. (2011). Effect of media-induced social distancing on disease transmission in a two patch setting. *Mathematical Biosciences, 230*, 87–95. https://doi.org/10.1016/j.mbs.2011.01.005
Tchoumi, S. Y., Rwezaura, H., & Tchuenche, J. M. (2022). Dynamic of a two-strain COVID-19 model with vaccination. *Results in Physics, 39*, Article 105777. https://doi.org/10.1016/j.rinp.2022.105777
Thompson, M. G., Burgess, J. L., Naleway, A. L., et al. (2021). Interim estimates of vaccine effectiveness of BNT162b2 and mRNA-1273 COVID-19 vaccines in preventing SARS-CoV-2 infection among health care personnel, first responders, and other essential and frontline workers - eight U.S. locations, 2020-2021. *MMWR Morb Mortal Wkly Rep, 70*, 495–500. https://doi.org/10.15585/mmwr.mm7013e3
van den Driessche, P., & Watmough, J. (2002). Reproduction numbers and sub-threshold endemic equilibria for compartmental models of disease transmission. *Mathematical Biosciences, 180*, 29–48. https://doi.org/10.1016/S0025-5564(02)00108-6
Vashishth, A. K., & Basaiti, K. (2024). Modeling the effect of non-pharmaceutical measures and vaccination on the spread of two variants of COVID-19 in India. *Mathematics and Computers in Simulation, 217*, 139–168. https://doi.org/10.1016/j.matcom.2023.10.008
Wang, W. (2022). Competitive exclusion of two viral strains of COVID-19. *Infectious Disease Modelling, 7*, 637–644. https://doi.org/10.1016/j.idm.2022.10.001
Wang, Q., Xiang, K., Zhu, C., & Zou, L. (2023). Stochastic SEIR epidemic models with virus mutation and logistic growth of susceptible populations. *Mathematics and Computers in Simulation, 212*, 289–309. https://doi.org/10.1016/j.matcom.2023.04.035
Wei, F., Zhou, R., Jin, Z., Huang, S., Peng, Z., Wang, J., et al. (2023). COVID-19 transmission driven by age-group mathematical model in Shijiazhuang City of China. *Infectious Disease Modelling, 8*, 1050–1062. https://doi.org/10.1016/j.idm.2023.08.004
World Health Drganization. (2020). Timeline: WHO's COVID-19 response. https://www.who.int/emergencies/diseases/novel-coronavirus-2019/interactive-timeline.
World Health Drganization. (2024). WHO COVID-19 dashboard. https://data.who.int/dashboards/covid19/cases.
Yan, Q., Tang, S., & Xiao, Y. (2018). Impact of individual behaviour change on the spread of emerging infectious diseases. *Statistics in Medicine, 37*, 948–969. https://doi.org/10.1002/sim.7548

Yu, B., Li, Q., Chen, J., & He, D. (2023). The impact of COVID-19 vaccination campaign in Hong Kong SAR China and Singapore. *Infectious Disease Modelling, 8*, 101–106. https://doi.org/10.1016/j.idm.2022.12.004

Zhai, X., Li, W., Wei, F., & Mao, X. (2023). Dynamics of an HIV/AIDS transmission model with protection awareness and fluctuations. *Chaos, Solitons & Fractals, 169*, Article 113224. https://doi.org/10.1016/j.chaos.2023.113224

Zhang, Y., & Xiao, Y. (2020). Global dynamics for a Filippov epidemic system with imperfect vaccination. *Nonlinear Analysis: Hybrid Systems, 38*, Article 100932. https://doi.org/10.1016/j.nahs.2020.100932

Zhao, S., Wang, K., Chong, M. K. C., Musa, S. S., He, M., Han, L., et al. (2022). The non-pharmaceutical interventions may affect the advantage in transmission of mutated variants during epidemics: A conceptual model for COVID-19. *Journal of Theoretical Biology, 542*, Article 111105. https://doi.org/10.1016/j.jtbi.2022.111105

Zhuang, C., Liu, X., Chen, Q., Sun, Y., Su, Y., Huang, S., et al. (2022). Protection duration of COVID-19 vaccines: Waning effectiveness and future perspective. *Frontiers in Microbiology, 13*, Article 828806. https://doi.org/10.3389/fmicb.2022.828806

Zou, Z., Fairley, C. K., Shen, M., Scott, N., Xu, X., Li, Z., et al. (2022). Critical timing and extent of public health interventions to control outbreaks dominated by SARS-CoV-2 variants in Australia: A mathematical modelling study. *International Journal of Infectious Diseases, 115*, 154–165. https://doi.org/10.1016/j.ijid.2021.11.024

Zou, Y., Huang, D., Jiang, Q., Guo, Y., & Chen, C. (2022). The vaccine efficacy against the SARS-CoV-2 Omicron: A systemic review and meta-analysis. *Frontiers in Public Health, 10*, Article 940956. https://doi.org/10.3389/fpubh.2022.940956